UNIVERSIDADE FEDERAL DE MINAS GERAIS

Instituto de Ciências Exatas

Programa de Pós-graduação em Física

Túlio Victor de Oliveira

Transition-metal monochalcogenide nanowires: Electron states and modulation of electronic properties

Belo Horizonte

2025

Túlio Victor de Oliveira

Transition-metal monochalcogenide nanowires: electron states and modulation of electronic properties

Tese apresentada ao Programa de Pós-Graduação em Física do Instituto de Ciências Exatas da Universidade Federal de Minas Gerais como requisito parcial para obtenção do título de Doutor em Ciências.

Orientador(a): Mario Sérgio de Carvalho Mazzoni

Coorientador(a): Guilherme Almeida Silva Ribeiro

Belo Horizonte

2025

Dados Internacionais de Catalogação na Publicação (CIP)

O48t Oliveira, Túlio Victor de.
Transition-metal monochalcogenide nanowires: electron states and modulation of electronic properties / Túlio Victor de Oliveira. – 2025.
53 f. : il.

Orientador: Mario Sergio de Carvalho Mazzoni.
Coorientador: Guilherme Almeida Silva Ribeiro.
Tese (doutorado) – Universidade Federal de Minas Gerais, Departamento de Física.
Bibliografia: f. 48-53.

1. Estrutura eletrônica. 2. Nanofios. 3. Teoria do Funcional da Densidade. I. Título. II. Mazzoni, Mario Sergio de Carvalho. III. Ribeiro, Guilherme Almeida Silva. IV. Universidade Federal de Minas Gerais, Departamento de Física.

CDU – 539.2 (043)

Ficha catalográfica elaborada por Romário Martins Ribeiro – CRB6 3595
Biblioteca Professor Manoel Lopes de Siqueira – Departamento de Física - UFMG

UNIVERSIDADE FEDERAL DE MINAS GERAIS

INSTITUTO DE CIÊNCIAS EXATAS

COLEGIADO DO CURSO DE PÓS-GRADUAÇÃO EM FÍSICA

FOLHA DE APROVAÇÃO

A presente tese, intitulada **"Transition metal monochalcogenide nanowires: Electron states and modulation of electronic properties",** de autoria de **TÚLIO VICTOR DE OLIVEIRA** submetida à Comissão Examinadora, abaixo-assinada, foi aprovada para obtenção do grau de **DOUTOR EM CIÊNCIAS, área de concentração Física ,** em vinte e quatro de outubro de 2025.

Belo Horizonte, 24 de outubro de 2025.

Prof. Mario Sérgio de Carvalho Mazzoni
Orientador do estudante
Departamento de Física/UFMG

Dr. Guilherme Almeida Silva Ribeiro
Coorientador do estudante

Prof. Ângelo Malachias de Souza
Departamento de Física/UFMG

Prof. Von Braun Nascimento
Departamento de Física/UFMG

Prof. André Alves Lino
Departamento de Física/UFPI

Prof. Ronaldo Júnio Campos Batista
Departamento de Física/UFOP

Documento assinado eletronicamente por **Guilherme Almeida Silva Ribeiro**, **Usuário Externo**, em 28/10/2025, às 15:43, conforme horário oficial de Brasília, com fundamento no art. 5º do Decreto nº 10.543, de 13 de novembro de 2020.

Documento assinado eletronicamente por **Von Braun Nascimento**, **Professor do Magistério Superior**, em 28/10/2025, às 16:11, conforme horário oficial de Brasília, com fundamento no art. 5º do Decreto nº 10.543, de 13 de novembro de 2020.

Documento assinado eletronicamente por **André Alves Lino**, **Usuário Externo**, em 28/10/2025, às 16:47, conforme horário oficial de Brasília, com fundamento no art. 5º do Decreto nº 10.543, de 13 de novembro de 2020.

Documento assinado eletronicamente por **Mario Sergio de Carvalho Mazzoni**, **Membro**, em 28/10/2025, às 22:04, conforme horário oficial de Brasília, com fundamento no art. 5º do Decreto nº 10.543, de 13 de novembro de 2020.

Documento assinado eletronicamente por **Angelo Malachias de Souza**, **Membro de comissão**, em 28/10/2025, às 23:48, conforme horário oficial de Brasília, com fundamento no art. 5º do Decreto nº 10.543, de 13 de novembro de 2020.

Documento assinado eletronicamente por **Ronaldo Júnio Campos Batista**, **Usuário Externo**, em 30/10/2025, às 10:13, conforme horário oficial de Brasília, com fundamento no art. 5º do Decreto nº 10.543, de 13 de novembro de 2020.

A autenticidade deste documento pode ser conferida no site https://sei.ufmg.br/sei/controlador_externo.php?acao=documento_conferir&id_orgao_acesso_externo=0, informando o código verificador **4676675** e o código CRC **8A2DC16F**.

Referência: Processo nº 23072.265405/2025-18 SEI nº 4676675

AGRADECIMENTOS

Primeiramente, agradeço à minha família por todo o suporte ao longo da vida. Em especial à minha mãe, dona **Malu**, e aos meus avós, dona **Maria José** e o "Seu" **Bené**. Sem eles, nada disso seria possível. Agradecimento especial à tia **Marcela** por todo suporte especialmente nos últimos tempos.

Meu agradecimento especial à **UFV-campus Florestal**, que me formou como professor de Física e me deu diversas oportunidades enquanto estudante, monitor, pesquisador e professor. Durante o doutorado me deram também a honra de ministrar um curso de estrutura eletrônica na Semana da Física que acontece no campus. Obrigado por tanto.

Falando em Florestal, preciso agradecer novamente à meus irmãos de vida e jornada: **República Irmandade4**. Aproveito para agradecer **Os Meninos**, que conheci em Florestal, e que tem me apoiado e dado suporte desde então, especialmente ao longo da estadia em BH. Ainda em BH, preciso agradecer imensamente a **Vaninha**, dona do **Bar do Cabral**, pela paciência de ouvir minhas lorotas e desabafos.

Agradeço aos estudantes de Física da UFMG pelo apoio ao longo do doutorado, em especial aos componentes da sala G1 pela paciência de dividir sala comigo. Tenho certeza que esqueci de citar muitas pessoas. Portanto, fica meu agradecimento geral a todos que contribuíram de alguma forma nessa jornada. Obrigado ao departamento de Física por todo suporte estrutural.

Agradeço também ao meu coorientador **Guilherme**, por todos os conselhos e apoio ao longo do mestrado e doutorado. Por fim, deixo o agradecimento ao **Mário** pela paciência, resiliência e os mais diversos ensinamentos. Agradeço também à banca avaliadora por aceitar o convite para contribuir com esse trabalho.

Agradeço à UFMG, FAPEMIG, CAPES e CNPq pelo suporte e apoio financeiro para o desenvolvimento desse trabalho.

RESUMO

Este trabalho versa sobre as propriedades eletrônicas de nanofios de monocalcogenetos de metais de transição, como MoTe, WTe, MoSe, MoS. Essas estruturas foram sintetizadas recentementes em experimentos que mostraram que podem se arranjar como estruturas bidimensionais, tridimensionais ou como fios isolados. Estudos têm mostrado rica fenomenologia associada às suas propriedades. Nesta tese, investigamos o problema do ponto de vista de métodos teóricos de primeiros princípios baseados no formalismo da Teoria do Funcional de Densidade. Em um primeiro momento, mostramos a versatilidade dos fios, que podem ser metais ou semicondutores de variados gaps de energia, podem ser manipulados para se comportarem como pontos quânticos, podem sofrer transiçoes metal-semicondutor induzidas por deformações, e podem se comportar de forma diversa de acordo com o tipo de substrato. Em um segundo tópico, mostramos como os fios podem se organizar em redes específicas, formando, por exemplo, estrutura tipo Kagomé ou hexagonal, e como isso leva às idiossincracias observadas nessas redes, como bandas "flat"e cones de Dirac.

Palavras-chave: Estrutura Eletrônica; nanofios; TMM; DFT; kagome; flatband

ABSTRACT

This work addresses the electronic properties of transition metal monochalcogenide nanowires, such as MoTe, WTe, MoSe, and MoS. These structures were recently synthesized in experiments that demonstrated that they can be arranged as two-dimensional, three-dimensional structures, or as isolated wires. Studies have demonstrated rich phenomenology associated with their properties. In this thesis, we investigate the problem from the perspective of first-principles theoretical methods based on the formalism of Density Functional Theory. First, we demonstrate the versatility of these wires, which can be metals or semiconductors with varying energy band gaps, can be manipulated to behave as quantum dots, can undergo deformation-induced metal-semiconductor transitions, and can behave differently depending on the substrate. In a second topic, we show how the wires can organize themselves into specific networks, forming, for example, a Kagome or hexagonal structure, and how this leads to the idiosyncrasies observed in these networks, such as "flat" bands and Dirac cones.

Palavras-chave: Electronic Structure; nanowires; TMM; DFT; kagome; flatband

SUMÁRIO

1 INTRODUCTION

A general feature in nanoscience development is the intense scrutiny of specific materials following significant advances in their syntheses and manipulation techniques. Invariably, the result is the unveiling of intriguing electronic behavior which moves forward basic science and paves the way for applications in nanotechnology. Recently, experimental reports have put one-dimensional (1D) transition-metal monochalcogenides (TMM) as candidates to play a central role in the nano research scenario, particularly in the rapidly expanding field of nanowires [1–4]. A TMM nanowire, as shown in Fig.1, consists of an one-dimensional structure containing sequential and inverted triangles of MX, where M is the metal (Cr, Mo, W) and X is the chalcogen (S, Se, Te). The latter atoms occupy the vertices of each triangle, while the metals occupy the midpoint of a line connecting the vertices of the triangle.

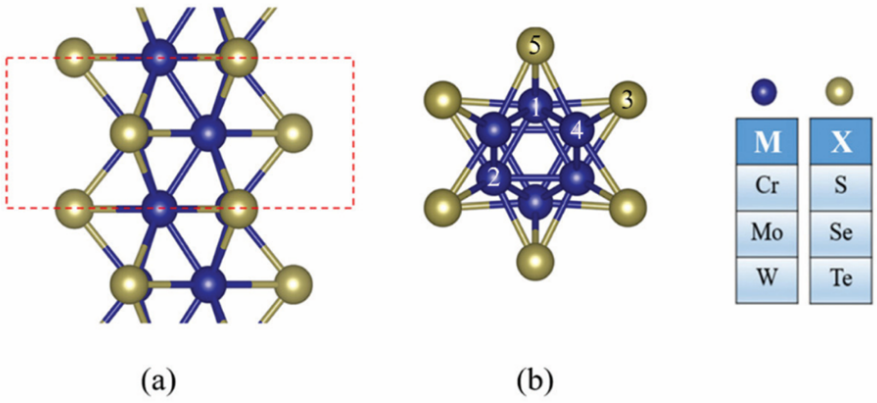

Figura 1 – (a) Side and (b) top views of the isolated MX nanowire crystal lattice. The unit cell is outlined by a dashed rectangle. Blue spheres denote metal atoms, and yellow spheres denote chalcogen atoms. Extracted from Zhang et al. [4]

Theoretical studies, using density functional theory (DFT) on TMM nanowires early revealed their structural stability. The pioneering work by Vilfan, in 2006, demonstrated mechanical robustness and electronic conductivity of Mo_6S_6 nanowires [5], establishing a conceptual foundation for subsequent investigations. Subsequently, ab initio calculations confirmed the stability of MoSe and MoS nanowires, with formation energies on the order of 1 eV/atom and metallic behavior [6]. These results promoted investigations into chemical functionalization and structural control. Murugan et al. explored the assembly of nanowires from tetrahedral Mo–S clusters and the effects of iodine doping on the electronic structure [7]. Subsequently, they investigated lithiated assemblies of Mo_6X_6 (X = S, Se, Te) nanowires, demonstrating structural stability and promising conductivity for applications as cathode materials [8]. More recent theoretical studies have significantly expanded the scope of investigated systems, addressing nanowires with different metallic and halogenated compositions, in addition to exploring emerging properties such as bifunctional catalysis, flexible electronics, and spin effects. Zhang et al. (2020) demonstrated that TMM nanowires act as highly efficient catalysts for oxygen evolution and reduction reactions,

with promising performance in electrochemical applications [4]. Shang et al. (2021) reviewed the TMM nanowire family as 1D materials for flexible electronics and spintronics, highlighting the structural and functional diversity of these systems [9].

In fact, following this early theoretical reports on the possible stability of monochalcogenide nanowires [6, 7] and their potential applications as cathode materials when intercalated with lithium [8], H. Zhu et al. described an experimental route to synthesize bundles of 1D MoTe compounds from 2H-$MoTe_2$ based on thermal activation under vacuum [10]. This transition, monitored by scanning transmission electron microscopy (STEM), is illustrated in Fig. 2, which comprises four panels taken directly from Zhu et al. [10]. Fig. 2(a) shows the transformation of 1D NWs of Mo_6Te_6 from 2H-$MoTe_2$. Energy-dispersive X-ray spectra (EDS) in Fig. 2(b) reveal a drop in the Te/Mo ratio from ≈ 1.87 in 2H-$MoTe_2$ to ≈ 1.07 inside the emerging bundles, confirming selective tellurium depletion and Mo_6Te_6 NW formation. The last panels in Fig. 2, c,d), present a time-series of Scanning Transmission Electron Microscopy - High Angle Annular Dark Field (STEM–HAADF) sectional views at 450 °C: the first captures the beginning of the nanowire piercing the $MoTe_2$, while the second follows their thermal stabilization under continuous heating, in addition to the formation of new nanowires. More recently, Liao et al. [11] used in situ STEM to unveil molybdenum-migration mechanism that drives this 2D-to-1D transformation.

TMMs nanowires are remarkably flexible at the sub-nanometer scale, allowing sharp bends, twists and branches. By precisely engineering defects and local stress, one can induce kinks, Y-junctions and X-junctions, paving the way for tailored one-dimensional nanowire architectures. In this scenario, Lin, J., Cretu, O., Zhou, W. et al. [12] employed a tightly focused electron beam to engineer TMM nanowires that interconnect discrete sites within a transition-metal dichalcogenide (TMD) monolayer. Additionally, J. Lin et al. [13] employed nanomanipulaton techniques to tune the structure of MoSe nanowires, producing Se vacancies, kinks, junctions and alloys. Fig. 3 illustrates each modification in three layers: experimental STEM images (top row), simulated STEM annular dark field images (middle row), and corresponding atomic models (top and side views, bottom row). Panel (A) revels a large twist induced by Se vacancies; panel (B) shows a kink which changes the axial direction; panel (C) depicts a branch where a secondary MoSe nanowire sprouts from the main strand; and panel D presents an X-junction interconnecting four MoSe nanowires.

A precise characterization of isolated nanowires was achieved by M. Nagata et al, [14], who stabilized them by encapsulation within carbon nanotubes (Fig. 4g)). Later, in 2021, employing the chemical vapor deposition (CVD) method, H. E. Lim et al [15] have shown how to build two- and three-dimensional lattices and assess their optical and electronic properties. The initially formed nanowire is used as a base to grow additional wires to form these lattices. According to these findings, the propensity to adopt sheet-like or bundle configurations is determined by whether wire–substrate interactions or wire–wire interactions dominate, respectively. Adjacent nanowires interact via van der Waals forces to self-assemble into 2D atomically thin sheets or

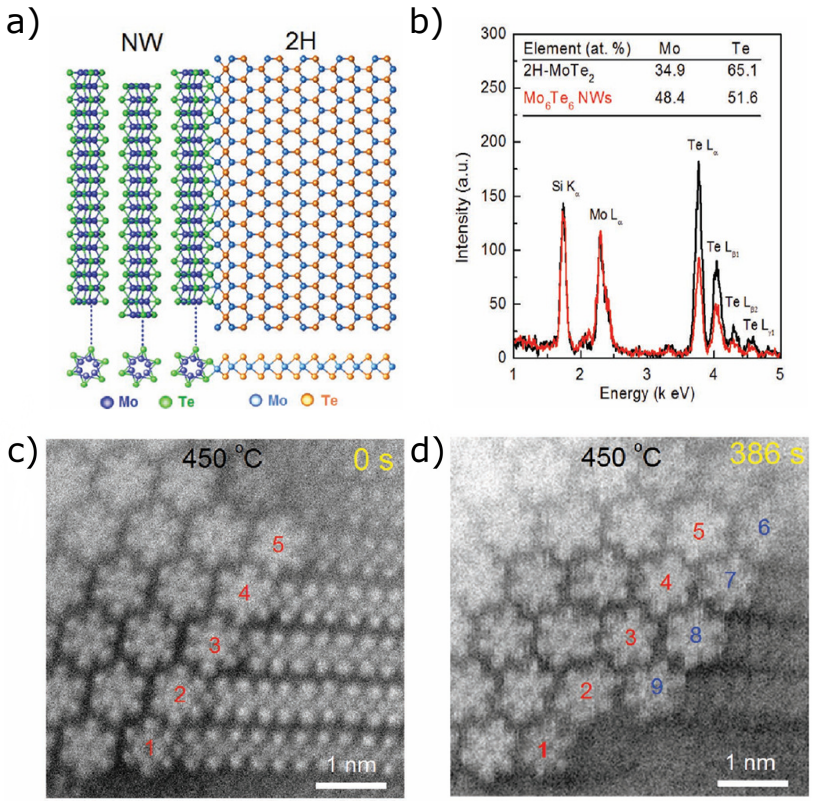

Figura 2 – Evolution and formation of Mo_6Te_6 nanowires from 2H-$MoTe_2$: a) Schematic depiction of the structural transformation converting layered 2H-$MoTe_2$ into sub-nanometer-diameter Mo_6Te_6 nanowires. (b) EDS spectra acquired on Mo_6Te_6 nanowire bundles and the neighboring 2H-$MoTe_2$ region, indicating Te/Mo ratios of 1.07 for the nanowires and 1.87 for the 2H phase. Silicon peaks arise from the SiC support film on the heating E-chip. (c,d) Time-series STEM-HAADF images showing the in situ nucleation and growth of new Mo_6Te_6 nanowires from 2H-$MoTe_2$. Adapted from Zhu et al. [10]

into 3D bundles of variable sizes. Fig 4a) schematically illustrates TMM isolated nanowires, 2D and 3D arrangments. Cross-sectional HAADF-STEM images in panels b) and c) confirm the formation of WTe monolayer and bilayer sheets grown on a-plane sapphire substrates, while panel d) reveals a representative 3D bundle structure formed on a SiO_2/Si surface. The internal structure of a single nanowire reveals a bright hexagonal ring of tungsten atoms enclosed by tellurium, as seen in Fig. 4 e), while atomic resolution imaging along the wire axis (Fig. 4 f) confirms the crystallographic periodicity and 1D character of these building blocks.

Based on this theoretical and experimental review, we will demonstrate the versatility of nanowires and the range of possible applications in which they can be useful. This thesis investigates transition-metal monochalcogenides subjected to various external factors capable of modulating or amplifying their properties. The scope of this work extends beyond isolated 1D nanowires to include ordered two- and three-dimensional arrays formed by these building blocks, enabling the exploration of collective phenomena that emerge from interwire coupling. First, we demonstrate how electronic, mechanical, and chemical properties can be deliberately tuned

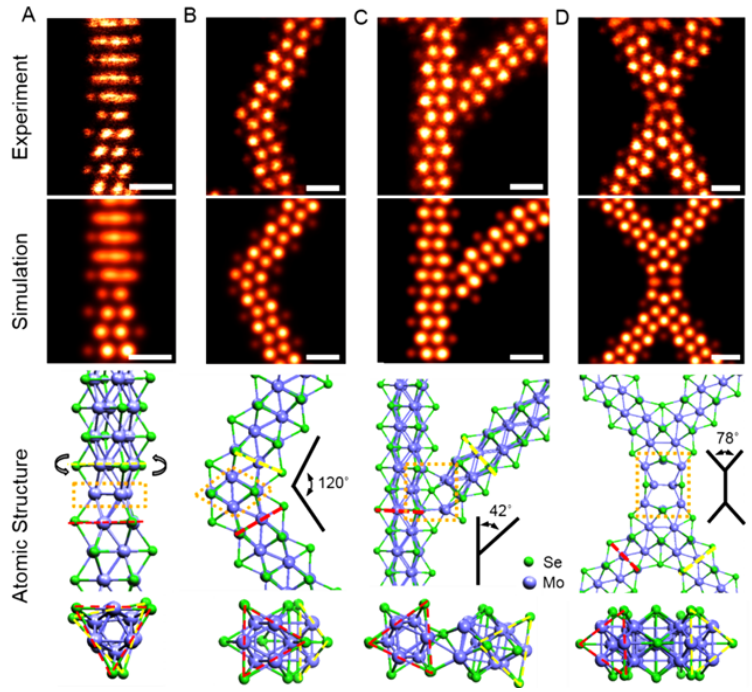

Figura 3 – Structural flexibility of MoSe nanowires. Panels (A-D) present, on first row, experimental Z-contrast STEM images, simulated annular fark-field STEM images on second row, and atomic models (top and side views, on third row) illustrating four distinct deformation modes: (A) a pronounced twist facilitated by Se vacancies, (B) a kink that redirects the nanowire's axis, (C) a branch where a secondary MoSe wire emerges and (D) an X-junction linking four nanowires. Adapted from J. Lin et al. [13]

through compositional changes, controlled doping, and the application of external strain. Next, we investigate interwire coupling - mediated by orbital hopping and van der Waals interactions - to understand how collective phenomena arise in three-dimensional networks. In particular, we focus on the emergence of flat band and Dirac cones driven by spin–orbit coupling. To achieve these goals, we employ a first-principles approach based on density functional theory (DFT) within the generalized gradient approximation (GGA) and norm-conserving pseudopotentials, performing structural relaxations, band-structure calculations, density-of-states analyses, and fatband projections.

In the following chapters, we systematically explore the theoretical and structural foundations of TMM nanowires and their emergent electronic behavior. Chapter 2 introduces the methodological framework, exploring the tight-binding model to interpret electronic features and density functional theory (DFT) for first-principles calculations. Chapter 3 presents a comprehensive characterization of different 1D wires, addressing their vast electronic structure, mechanical flexibility, response to external stresses and defects, and how the nanowires interact with potential substrates. Chapter 4 discusses the integration of MoTe nanowires into honeycomb and kagome lattice networks, highlighting the interplay between geometry and symmetry in engineered quantum systems. Finally, Chapter 5 presents the general conclusions, consolidating the key findings, and outlining prospects for future applications and theoretical extensions.

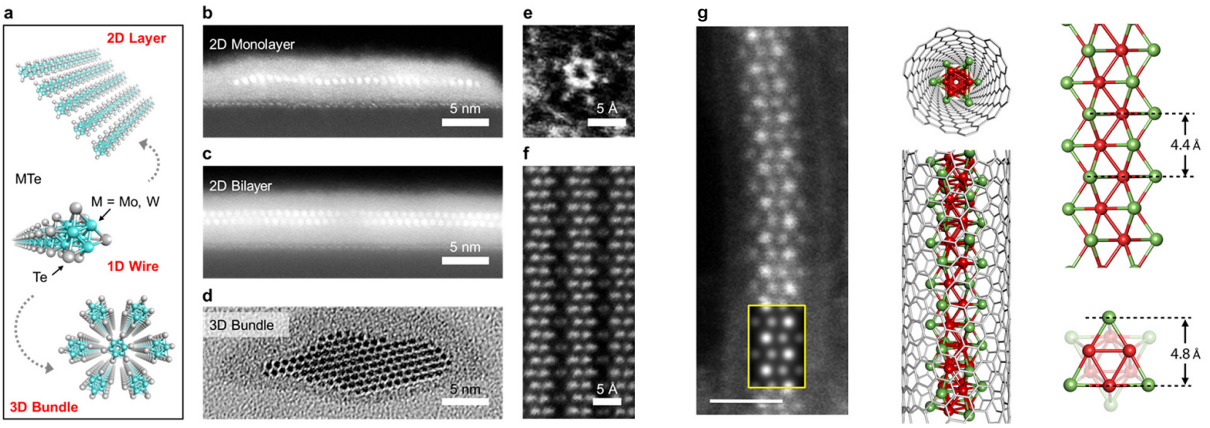

Figura 4 – 1D van der Waals building blocks. (a) A schematic diagram illustrating the 1D TMM nanowire, 2D and 3D architectures from TMMs. (b, c) Cross-section HAADF-STEM images of monolayer and bilayer of WTe nanowire sheets grown on a-plane sapphire substrates. (d) Cross-section TEM image of a0 3D bundle of WTe nanowires deposites on a SiO_2/Si substrate. (e) HAADF-STEM cross-section of an individual WTe nanowire, in which the W core appears as a bright hexagonal ring surrounded by Te atoms. (f) Atomic resolution HAADF-STEM image of suspended WTe nanowires, showing their crystallographic alignment along the wire axis. (g) Experimental HAADF-STEM image of a single MoTe nanowire encapsulated inside a carbon nanotube, with the corresponding simulated image inset and the atomic-structure model alongside. (a-f) Adapted from Lim et al. [15]. (g) Adapted from Nagata et al. [14]

2 METHODS

In this chapter, we employ density functional theory (DFT), as implemented in SIESTA, as our primary computational tool to obtain accurate relaxed geometries, band structures, and densities of states (DOS) for TMM nanowire systems. These first-principles results are complemented by a tight-binding (TB) model, which provides an intuitive, symmetry-based interpretation of Dirac cones, flat bands, and orbital hybridization. Applied a posteriori to the DFT dispersions, the TB model highlights the key symmetry-driven features underlying the electronic behavior of nanowires embedded in honeycomb and kagome architectures. In the honeycomb lattice, exemplified by graphene, p_z orbitals hybridize to form dispersive bands and a Dirac cone; while the kagome lattice, which includes three orbitals per unit cell, yields similar dispersive bands along with a characteristic flat band.

Section 2.1 introduces the formalism of the TB model and its application to the honeycomb lattice - where p_z orbitals yield Dirac cones - and to the kagome lattice, which features both dispersive bands and a flat band. In Section 2.2 we present the details of our DFT/SIESTA calculations, including pseudopotentials and basis sets. Finally, Section 2.3 summarizes how this combined DFT + TB framework yields a consistent, physically grounded picture of low-dimensional electronic behavior and prepares the ground for the nanowire-decorated lattices studied in Chapters 3 and 4.

2.1 Tight-binding model

The tight-binding (TB) model represents single-particle electronic states as linear combinations of localized atomic orbitals. This approach is particularly useful for capturing the symmetry-driven features of low-dimensional systems such as TMM nanowires. Bloch's Theorem

$$\Phi_{nk}r \;\; R = e^{ik\cdot R}\Phi_{nk}r \tag{2.1}$$

ensures translational invariance in a crystal with Bravais lattice vectors R. We build Bloch's sums $\Phi_j k, r$

$$\Phi_j k, r = \frac{1}{N} \sum_{R} e^{ik\cdot r}\, \phi_j r - R \tag{2.2}$$

to exactly satisfy this condition. The *j* index representing the atomic orbitals belonging to the primitive cell and N the number of primitive cells. With this bases, the Hamiltonian matrices elements $H_{jj'}k$ and the overlap matrices elements $S_{jj'}k$ are

$$H_{jj'}k = \langle \phi_j | \hat{H} | \phi_{j'} \rangle \qquad , \qquad S_{jj'}k = \langle \phi_j | \phi_{j'} \rangle$$

Here, two parameters carry clear physical meaning:

- Onsite energy $\varepsilon_j = H_{jj}$: the energy of an electron located at site j, without interaction with neighboring atoms. For simplicity, this value is often set to zero to isolate the effects of inter-site interactions.

- Hopping integral $t_{jj'} = H_{jj'}$, for $j \neq j'$: measures the amplitude for an electron to "hop" between neighboring sites and controls band widths and dispersion slopes.

Applying the variational principle to the energy E_i, which defines the electronic band structure, yields the secular equation

$$\det[H_{jj'}k - E * S_{jj'}k] = 0\,. \tag{2.3}$$

Thus, the secular condition (in matrix form: $\det H - ES = 0$) encapsulates how on-site energies, hopping integrals, and orbital overlaps together dictate the allowed energy eigenvalues $E\mathbf{k}$ and hence the full band dispersion. With this formal framework in hand, we now turn to its concrete realization in two 2D networks: first, the honeycomb lattice - a bipartite hexagonal array of p_z orbitals whose nearest-neighbor hoppings give rise to Dirac cones at the Brillouin-zone K points - and then the kagome lattice, whose three-site basis supports both dispersive Dirac-like bands and a symmetry-protected flat band arising from destructive interference.

2.1.1 Honeycomb lattice

The honeycomb lattice, shown in Fig.6, has two atoms (A and B) per unit cell, each contributing one orbital (such as p_z in graphene) in the simplest case. The three nearest-neighbor vectors n_1, n_2, n_3 connect A and B. The 2×2 tight-binding Hamiltonian reads

$$\hat{H} = \begin{pmatrix} H_{AA} & H_{AB} \\ H_{BA} & H_{BB} \end{pmatrix} = \begin{pmatrix} \varepsilon & -t\,\gamma k \\ -t\,\gamma^* k & \varepsilon \end{pmatrix}, \qquad \gamma k = e^{ik\cdot n_1}\ e^{ik\cdot n_2}\ e^{ik\cdot n_3}\,.$$

Figura 5 – Honeycomb lattice showing sublattices A and B and nearest-neighbor vectors. [16]

Diagonalizing Hk, from the secular equation, yields the band energies

$$Ek = \pm\, t\,|\gamma k|\,.$$

The dispersive bands are shown in Fig. 6, whose Brillouin Zone is also hexagonal, with Γ, K and M as points of high symmetry in the reciprocal lattice. Therefore, a hexagonal lattice

compound for two orbitals (one at each atomic site) presents two dispersive bands, whose widths are proportional to the hoppings among first neighbors in the network and a function γ dependent on the wave vector k.

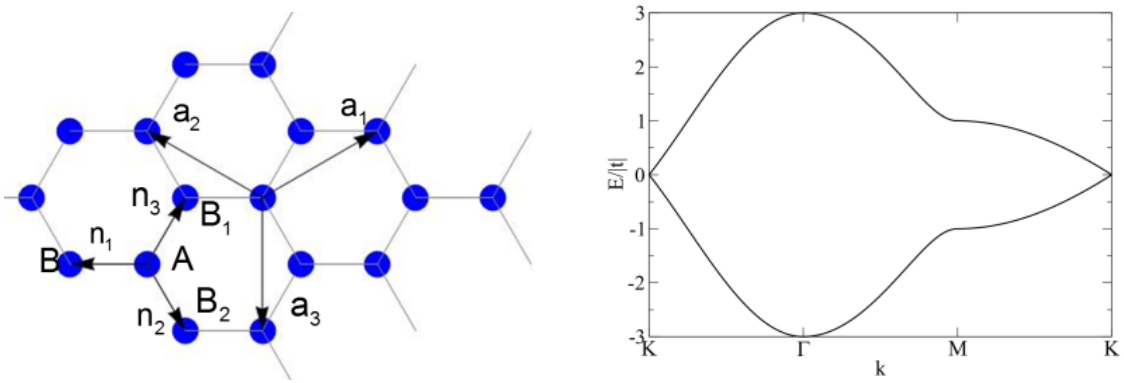

Figura 6 – Left panel: honeycomb lattice showing sublattices A and B and nearest-neighbor vectors. Right panel: tight-binding band structure of the honeycomb lattice showing two dispersive bands and Dirac cones at K point. Extracted from reference [16]

Once the honeycomb lattice formalism established, we now proceed in next section to the kagome lattice, where a three-site basis yields both dispersive and symmetry-protected flat bands.

2.1.2 Kagome lattice

The kagome lattice, shown in Fig. 7, is built on a triangular Bravais net with three sites per unit cell, forming corner-sharing triangles. In the simplest tight-binding description each site contributes one orbital and only nearest-neighbor hoppings t are included. We choose to label the three sublattices as 1, 2 and 3. In this case, every atom has four neighboring atoms, i.e., we need to explicit four vectors to connect the atom 1 to its neighbors 2 and 3:

$$v_{12} = \frac{\sqrt{3}}{4} a\,\hat{i} - \frac{1}{4} a\hat{j} \quad ; \quad v_{1\bar{2}} = -\frac{\sqrt{3}}{4} a\,\hat{i}\ \frac{1}{4} a\hat{j} = -v_{12}$$

$$v_{13} = \frac{\sqrt{3}}{4} a\,\hat{i}\ \frac{1}{4} a\hat{j} \quad ; \quad v_{1\bar{3}} = -\frac{\sqrt{3}}{4} a\,\hat{i} - \frac{1}{4} a\hat{j} = -v_{13}$$

The index 12 means that the vector connects atoms 1 and 2. As honeycomb lattice, the elements of the main diagonal of 3×3 Hamiltonian are the onsite terms:

$$H_{11} = H_{22} = H_{33} = \varepsilon\,.$$

The non-diagonal elements depend on the hopping matrix elements between the first neighbors t, and exponential functions with scalar products between the wave vectors k and the vectors connecting the first neighbors. So, the Hamiltonian that describes the kagome lattice with one orbital per atomic site is

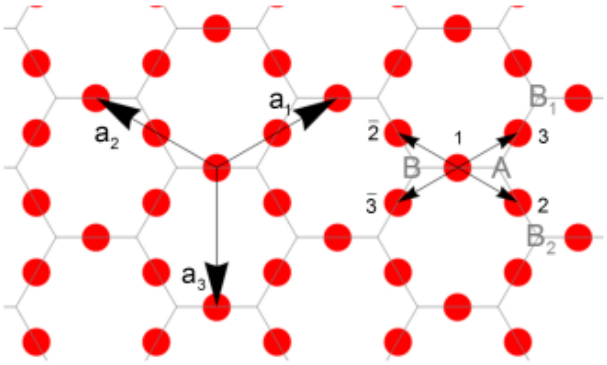

Figura 7 – Kagome lattice. [16]

$$H = \begin{pmatrix} \varepsilon & -2t\ \cos K_1 & -2t\ \cos K_2 \\ -2t\ \cos K_1 & \varepsilon & -2t\ \cos K_3 \\ -2t\ \cos K_2 & -2t\ \cos K_3 & \varepsilon \end{pmatrix} .$$

For simplicity, the scalar products mentioned above were defined as

$$k \cdot v_{12} \equiv K_1 \ , \ k \cdot v_{13} \equiv K_2 \ , \ k \cdot v_{13} - v_{12} \equiv K_3 \, .$$

Diagonalizing the secular equation yields one flat band and two dispersive bands:

- Flat band:

$$E = -2t \, ,$$

which is independent of k and arises from destructive interference aroud each triangle.

- Dispersive bands:

$$E_{\pm} = t\ 1 \pm |Sk| \, ,$$

with

$$Sk = \cos 2K_2\ \cos 2K_2\ \cos 2K_3 \, .$$

As shown in Fig. 8, in the kagome lattice the electronic structure in characterized by the flat band an by two sets of dispersive Dirac bands. In real materials, the situation becomes more involved, since long-range interactions, which require inclusion of next-neighbor hoppings, may affect quantum interference and induce dispersion in the flat band [17]. In addition, realistic cases usually correspond to multiorbital systems with multiple hoppings [18]. In CoSn, for instance [19, 20], Co atoms form a kagome-like lattice with different sets of flat bands derived from d-states. This scenario may also appear in other lattices. That is the case for graphene lattices with the choice of in-plane p_x,p_y orbitals when they are well separated from s orbitals. When the s-p hybridization is avoided, as in some optical lattices, the result is the emergence of flat bands touching the Dirac bands [21, 22].

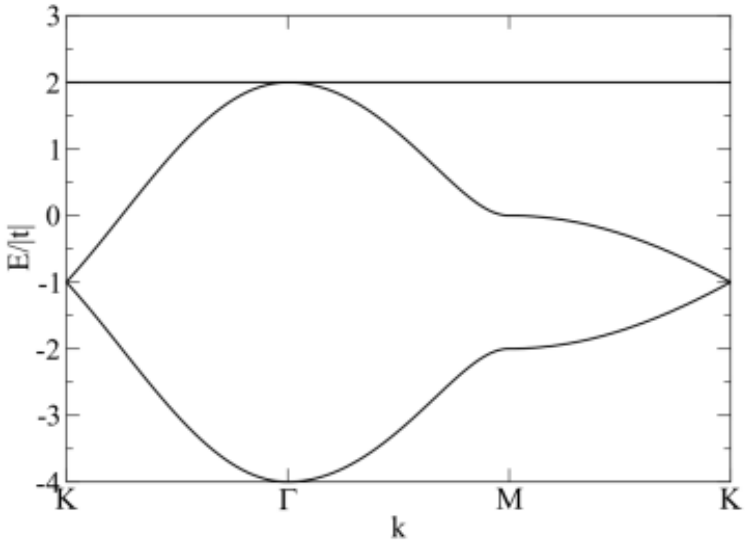

Figura 8 – Band structures referring to the TB model for the kagome lattice. [16]

2.1.3 $P_x - p_y$ honeycomb lattice

In honeycomb hexagonal lattices, similar to graphene, the p_z orbitals hybridize to form dispersive bands with Dirac cones at the K point of the Brillouin zone. Wu et al. proposed a tight-binding model for the p_x, p_y orbitals whose hoppings containing p_z orbitals are ignored [21,22]. In this p_x, p_y-model there are additional scalar products to the hopping t between neighboring sites, since the p_x and p_y orbitals are not always aligned with the vectors connecting the neighboring sites. There are four orbitals involved in the model (two per atomic site), so that we obtain four energy bands. It can be shown [16] that a possible solution leads to two dispersive bands with Dirac cones ($E_{2,3}$) and two flat bands ($E_{1,4}$), one above and one below the dispersive bands, touching them at the point Γ:

$$E_{2,3} = \pm\frac{|t|}{2}|\gamma K\,;$$

$$E_{1,4} = \pm\frac{3|t|}{2}\,.$$

These bands are shown in Fig. 9.

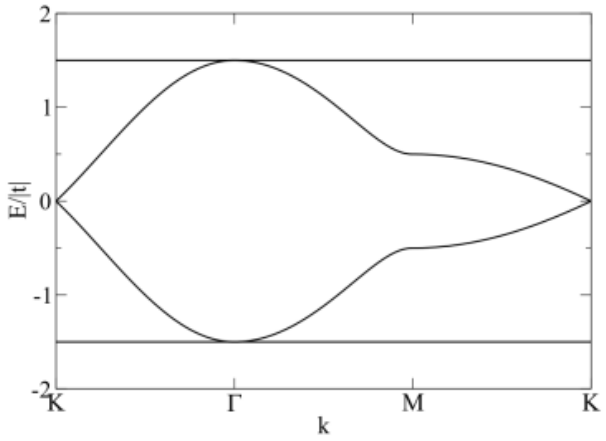

Figura 9 – Band structures referring to the TB model for the honeycomb lattice to the p_x and p_y orbitals. [16]

2.2 Density Functional Theory

Density Functional Theory (DFT) is widely used and powerful approach to treating quantum systems. DFT offers a first-principles route to the ground-state energy and density of an interacting many-electron system by replacing the full wavefunction

$$\Psi r_1, r_2, ..., r_N$$

with the electron density nr. This reduction - from $3N$ variables to just 3 - makes large-scale calculations tractable while retaining solid accuracy for geometry relaxation, band structure and density of states analyses.

So, we just need to know the electron density of the system to determine the wave function and the external potential vr and, consequently, the observables of interest. In this theory, any property of the ground state of a system of interacting electrons is a functional of the ground state electron density n_0:

$$F = Fn_0 \, .$$

2.2.1 Theoretical Foundations

DFT is grounded in two theorems by Hohenberg-Kohn [23]:

- **Unique mapping:** The ground-state electron density n_0r of a system of interacting electrons in an external potential field vr uniquely determines this potential, i.e.

  $$vr = vn_0r \, .$$

  As a consequence of this first theorem, all properties of the system will be determined given the density of the ground state. Therefore, the total energy of the system becomes a functional of the density:

  $$En = \langle \psi n | \hat{T} \;\; \hat{U} \;\; \hat{V} | \psi n \rangle, \, .$$

- **Variational principle:** There is a universal functional for the energy En that can be defined for any external potential vr. The energy functional En is minimal for the exact ground-state electron density n_0r.

To calculate the ground-state electron density, Kohn and Sham [24] proposed an ansatz that simplifies the many-interacting-body problem. To do so, the idea is to replace the original

problem of interacting electrons with an auxiliary problem of independent electrons, both with the same electron density. The Hamiltonian of the auxiliary system is chosen as having a usual kinetic energy operator and an effective potential V_{ef} acting on each electron of the non-interacting system. This auxiliary system allows us to obtain single-particle states that will be important for determining the electron density. Through the ansatz, therefore, we can obtain the Khon-Sham equations.

Let E be the total energy of the system of interacting electrons given by the sum of the kinetic energy T of the electrons, the electron-electron interaction energy U and the nucleus-electron interaction energy V:

$$E = T\ U\ V\,.$$

As we already know, energy is a functional of density. Therefore, the kinetic energy will also be. Let's separate into two terms: the kinetic energy of the non-interacting system T_s and the portion of the kinetic energy due to the interaction between the electrons T_c:

$$T = Tn = T_s n\ T_c n\,.$$

Something similar can be done for the electron-electron interaction energy, formed by the Hartree energy U_H, the exchange energy U_x and the energy due to the electronic correlation U_c:

$$U = Un = U_H n\ U_x n\ U_c n\,.$$

So, for the energy functional we have:

$$En = T_s n\ T_c n\ U_H n\ U_x n\ U_c n\ Vn\,.$$

We define the correlation and exchange functional $E_{xc}n$:

$$E_{xc}n = T_c n\ U_x n\ U_c n\,,$$

whose form is not known and we treat it through approximations. Therefore, everything we do not know about the effects of correlation and exchange between the electrons in our system is contained in this functional. The energy is rewritten as:

$$En = T_s n\ U_H n\ Vn\ E_{xc}n\,.$$

To determine the Kohn-Sham equation, we first minimize the energy with respect to the density nr:

$$0 = \frac{\delta E}{\delta nr} = \frac{\delta T_S}{\delta nr}\ \frac{\delta U_H}{\delta nr}\ \frac{\delta V}{\delta nr}\ \frac{\delta E_{xc}}{\delta nr}\,,$$

$$0 = \frac{\delta T_S}{\delta nr}\ v_H r\ vr\ v_{xc} r\,.$$

Here, vr is the external potential acting on the electrons; $v_H r$ is simply the Hartree potential; and $v_{xc} r$ is a potential associated with the correlation and exchange energies E_{xc}.

Now, for a system of non-interacting particles moving in a potential $v_S \mathbf{r}$, the Hartree and xc terms are missing, making minimization simpler:

$$0 = \frac{\delta E}{\delta nr} = \frac{\delta T_S}{\delta nr} \; \frac{\delta V_S}{\delta nr} = \frac{\delta T_S}{\delta nr} \; v_S r \,,$$

Comparing their minimizations, if $v_S r$ is chosen

$$v_S r = v_H r \;\; vr \;\; v_{xc} r \,,$$

this gives us the same density for both systems $n_S r \equiv nr$. This equation for $v_S r$ is one of the Kohn-Sham equations.

Therefore, from the solution of the non-interacting system at a potential $v_S r$, we can calculate the electron density of the interacting system at the potential vr. That is,

$$nr \equiv n_s r = \sum_i^N f_i |\phi_i r|^2 \,.$$

This is the second Khon-Sham equation. In it, we define f_i as the i-th occupied orbital and ϕ_i as the orbitals produced by the solution of the Schoedinger equation of the auxiliary system,

$$\left[-\frac{\hbar^2}{2m} \nabla^2 \;\; v_s nr \right] \phi_i r = \epsilon_i \phi_i r \,. \tag{2.4}$$

2.2.2 SIESTA

All DFT calculations are performed with the SIESTA package [25], which combines a set of localized numerical basis sets with norm-conserving pseudopotentials and a representation of charge and potential in the real space grid. SIESTA solves the Kohn–Sham equations self-consistently for the orbitals $\{\phi_i\}$. SIESTA expands each Kohn–Sham orbital in a finite basis of atom-centered numerical functions $\{\chi_\mu\}$:

$$\phi_i \mathbf{r} = \sum_\mu C_{i\mu} \, \chi_\mu \mathbf{r} \,.$$

In this representation, the Kohn–Sham equations reduce to a generalized eigenvalue problem

$$\sum_\nu [H_{\mu\nu} - \varepsilon_i \, S_{\mu\nu}] \, C_{i\nu} = 0 \,,$$

with matrix elements

$$H_{\mu\nu} = \langle \chi_\mu | \; -\tfrac{\hbar^2}{2m} \nabla^2 \;\; v_s n | \chi_\nu \rangle \,,$$

and

$$S_{\mu\nu} = \langle \chi_\mu | \chi_\nu \rangle \, .$$

The electron density is reconstructed as

$$n\mathbf{r} = {}_i \, f_i \, |\phi_i \mathbf{r}|^2 = {}_{\mu\nu} \, P_{\mu\nu} \, \chi_\mu \mathbf{r} \, \chi_\nu \mathbf{r} \, ,$$

where $P_{\mu\nu} = {}_i \, f_i \, C_{i\mu} C^*_{i\nu}$ defines the density matrix. A real space grid, controlled by an energy cutoff, is used to assess Hartree and exchange-correlation potentials and charge density. The self-consistent cycle proceeds as follows:

- Initialize a trial density $n^0\mathbf{r}$,
- Build $v_s n^k$ and assemble $H_{\mu\nu}$,
- Solve the generalized eigenproblem for $\{C_{i\mu}\}$ and $\{\varepsilon_i\}$,
- Reconstruct $n^{k1}\mathbf{r}$ from the occupied states;
- Mix densities and repeat until total energy and forces converge.

Using norm-conserving pseudopotentials, SIESTA eliminates the need to explicitly treat core electrons while maintaining transferability between chemical elements. The localized basis in our study delivers accurate valence properties at a fraction of the cost of plane-wave methods. This combination of numerical efficiency and first-principles rigor underpins the reliable geometries, band structures, density of states and fatbands data that feed into our tight-binding analysis in Chapters 3 and 4.

3 ONE-DIMENSIONAL NANOWIRES

Transition-metal monochalcogenide nanowires exhibit remarkable electronic and structural versatility, manifesting in metallic and semiconducting forms depending on their composition and environment. These 1D systems can be synthesized through chemical vapor deposition (CVD) [15], encapsulation within carbon nanotubes [14], thermal transition of the 2D-TMD phase via vacuum annealing [10] [26], and by electron-beam irradiation of 2D-TMD [13]. Furthermore, the latter produced nanowires incorporating multiple chalcogenides atoms into their composition (such as MoS_xSe_{1-x} or $Mo_xW_{1-x}S$) derived from vertically stacked monolayers or heterostructures. This concept serves as the basis for investigating defects, such as a MoSe segment inserted into a MoTe nanowire, as will be discussed in this chapter. In addition, we demonstrate that strain significantly influences the electronic behavior of the MoSe nanowire. When subjected to approximately 10% strain, the nanowire undergoes a metal–semiconductor transition — a threshold comparable to that observed in certain transition metal dichalcogenides (TMDs). Finally, their band structures are highly sensitive to adjacent structures, making them ideal platforms for exploring quantum phenomena such as spin splitting, anisotropic charge distributions, and band reorganizations. By placing TMM nanowires close to functional materials — including semiconducting monolayers, neutral molecular supports, and 2D ferromagnets — it becomes possible to tailor their electronic behavior through substrate engineering and interfacial coupling. This chapter also examines the interaction involving of WTe nanowires with PtS_2, silane, and CrI_3, highlighting the role of proximity effects in shaping quantum functionalities. Our first-principles calculations were performed using DFT [23, 24] as implemented in SIESTA [25]. Norm-conserving pseudopotentials and a double-zeta polarized (DZP) basis were employed. Exchange–correlation effects were treated within the Generalized Gradient Approximation using the Perdew–Burke–Ernzerhof functional (GGA-PBE) [27]. The geometries were optimized with a tolerance in the maximum force component in any atom of 0.002 eV/Å. All calculations included spin polarization. The real-space grid for numerical integration was set using an energy cutoff of 450 Ry. The Brillouin zones were sampled using 1x1x20 k-mesh for all 1D nanowires and 30 Å for k-mesh cutoff in the interaction between nanowires with possible substrates.

3.1 Electronic structure of isolated nanowires

Monochalcogenide transition-metal (TMM) nanowires exhibit remarkable electronic versatility that depends on the choice of transition metal and chalcogen. Fig. 10 shows band structures and corresponding projected densities of states (PDOS) of MoTe, WTe, MoS and MoSe nanowires, with the Fermi level set to $E_F = 0\ eV$ (blue dashed line). A complete description of the interatomic distances and binding energies for important nanowires is provided by Çakir et al [6]. The bond lengths, extracted from our relaxed geometries, are in good agreement with those obtained by reference [6] and are presented below:

- **MoTe**: Mo-Te = 2.84 Å ; Mo-Mo = 2.68 Å
- **WTe**: W-Te = 2.89 Å ; W-W = 2.73 Å
- **MoS**: Mo-S = 2.52 Å ; Mo-Mo = 2.80 Å
- **MoSe**: Mo-Se = 2.64 Å ; Mo-Mo = 2.79 Å

MoTe nanowires display an indirect, narrow-gap semiconducting behavior with a band gap of approximately 0.2 eV. At the valence band maximum (VBM), in-plane Mo d-orbitals (d_{xy} and $d_{x^2-y^2}$ give rise to a pronounced PDOS peak around -0.1 eV, accompanied by a modest contribution from Te $5p_x$ and $5p_y$. At the conduction band minimum (CBM), the tellurium px and py orbitals dominate the DOS. WTe nanowires exhibit a similarly semiconducting character but with an even smaller gap of about 40 meV. The orbital decomposition closely parallels that of MoTe, except that the Te $5p_x$ and $5p_y$ play a slightly more prominent role in the conduction band near the Fermi level. This slight but significant shift underscores how varying the transition metal tunes the band structure.

In contrast, MoS and MoSe nanowires behave as genuine 1D metals, with multiple bands crossing the Fermi level. In both cases, the Mo $4d_z^2$ orbital dominates the region immediately above E_F, with secondary contributions from the chalcogen p_z orbitals, while the valence-band edge is governed by in-plane orbitals (Mo $d_{xy}d_{x^2-y^2}$ and chalcogen p_xp_y).

Further amplifying this electronic tunability, a recent study demonstrates that surface functionalization, atom doping, and strain engineering provide additional avenues to continuously modulate the band structure of TMM nanowires. These approaches can push their band gaps from metallic through narrow semiconductor regimes and even inducing magnetic transitions in certain compositions [9]. In summary, TMM nanowires offer an exceptional electronic duality: selecting sulfur or selenium yields metallic conduction, whereas tellurium incorporation opens narrow, tunable band gaps. This metal–semiconductor duality, together with precise control over band-gap width by choosing the chalcogen or transition metal, positions TMM nanowires as versatile platforms for one-dimensional devices. These characteristics make them suited for integrated nanoscale architectures. In the following, we will further explore this aspect presenting original situations which highlight the electronic versatility of TMMs.

3.2 MoTe - MoSe heterostructure

In the previous section, we explored four one-dimensional nanowires of transition metal monochalcogenides (TMMs): MoSe and MoS exhibited metallic behavior, while MoTe and WTe were semiconductors with a small energy gap. We now investigate a heterostructure

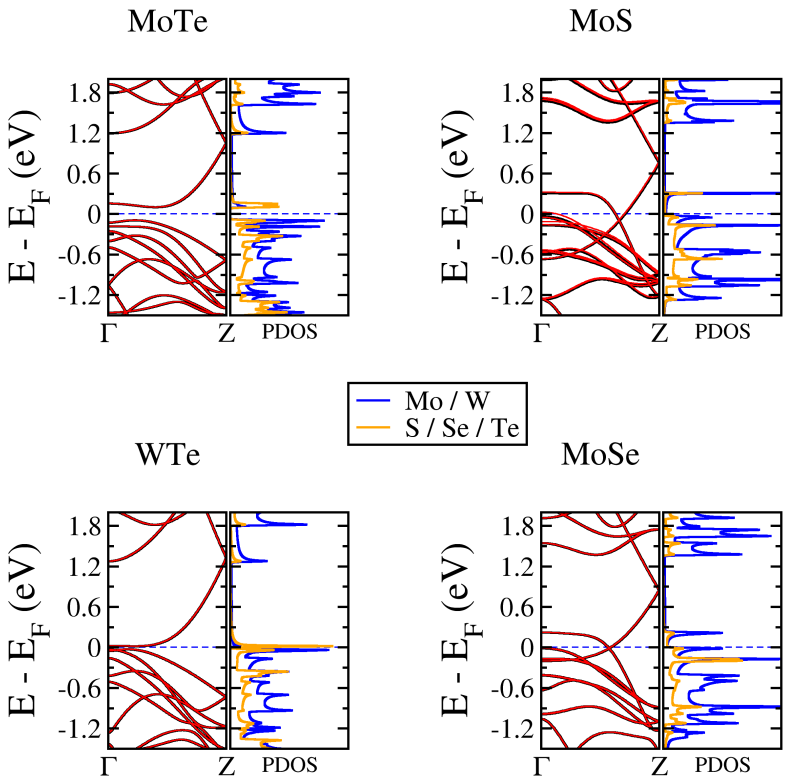

Figura 10 – Band structures of MoTe, WTe, MoS and MoSe nanowires and its respective projected density of states. In $\Gamma - Z$ path, red and black solid lines represent distinct spin components. Blue and orange solid lines, in PDOS panels, represent transition-metal (Mo or W) and chalcogen (S, Se or Te), respectively.

composed of a metallic MoSe segment embedded in a semiconducting MoTe matrix. The MoSe segment corresponds to three repetitions of the unit cell of an isolated nanowire, totaling 36 atoms (12 atoms per cell). In contrast, two configurations of the MoTe matrix are used: seven repetitions of MoTe triangles, totaling 84 atoms, and seventeen repetitions, totaling 204 atoms. The MoTe-MoSe heterostructure are shown in Fig. 11. The aim here is to assess whether these asymmetric configurations ensure a semiconductor region sufficiently extended to support electronic confinement, while maintaining a well-defined semiconductor domain, as present in the isolated MoTe nanowire, for comparison. The interface between these segments acts as a chemically and structurally modulated region where discrete electronic states emerge.

The feasibility of these chalcogenide substitutions is supported by experimental and theoretical evidence. Spectroscopic and DFT studies on TMDs show that controlled substitution of chalcogen atoms in MoX_2 (X = S, Se, Te) modifies band alignment and orbital hybridization. Wang, Chen, and Wu et al. [28] reviewed atomic substitution strategies in low-dimensional transition metal chalcogenides, including 1D systems, highlighting the impact of atomic substitution on band structure and morphology, which can influence electronic distribution in low-dimensional systems. Rehman et al. [29] conducted selective substitution experiments of Te by Se in $MoTe_2$, forming ternary alloys with tunable semiconducting behavior. Their experimental results showed

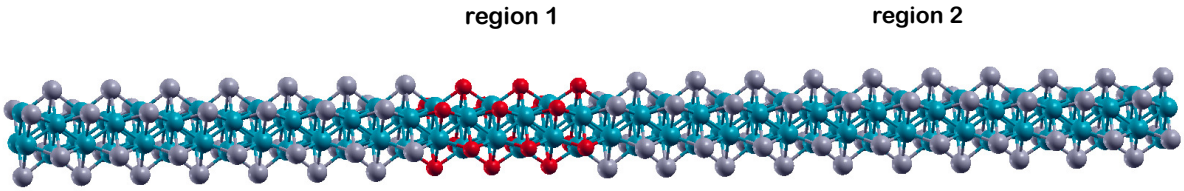

Figura 11 – Structute of a MoSe segment inserted into a semiconducting MoTe nanowire. Blue, gray and red spheres represent Mo, Te and Se, respectively.

that substitution modifies the electronic gap and charge distribution, thereby demonstrating the potential of chemical engineering to control electronic properties in low-dimensional systems. Although focused on 2D layers, their findings are relevant to confined segments in nanowires. These studies confirm that chemical modulations can alter electronic properties and provide conceptual support for the formation of discrete states in confined systems. Complementing these findings, Lin et al. [13] demonstrated experimentally that TMM nanowires can incorporate multiple chalcogen elements (S, Se, W) in controlled proportions, forming flexible multichalcogenide alloys. Using STEM and DFT, they showed that the chalcogen composition directly influences the electronic density of states and can be tuned via chemical alloying. This experimental evidence reinforces the feasibility of modulating the electronic structure of 1D TMM systems through chalcogen ratio engineering.

We now present band structures and the density of states (DOS) of the MoTe–MoSe heterostructure, which confirms that discrete peaks near the Fermi level emerge directly from the MoSe region when embedded in a MoTe nanowire. Two configurations were analyzed: a simple unit cell with 120 atoms and an expanded cell with 240 atoms, both containing a fixed defect of 36 MoSe atoms. Those systems were divided in two regions. Region 1 contains the MoSe defect, with the inclusion of the first MoTe atoms neighboring the defect to capture the effects at the interface between the wires, while region 2 is the remainder of the MoTe nanowire. The results indicate that some flat bands are present in the energy gap region, with emphasis on the two bands above the Fermi level. The presence of these discrete levels is attributed to the MoSe segment. To investigate this, we first examine the MoTe-MoSe nanowire containing 120 atoms, with band structure and total DOS per atom for each region presented in Fig. 12. In the DOS, we clearly see that region 1 dominates the discrete states belonging to the flat band in the energy gap (two highlighted bands above the Fermi level and two bands just below, in the range of approximately -0.05 eV).

The result already indicates that the emergence of discrete states inside the band gap can be unambiguously attributed to the defect. However, to avoid any distortions from a disproportionately

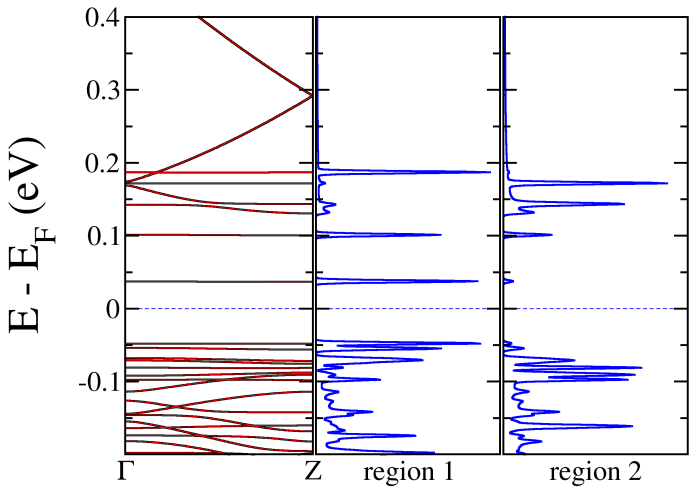

Figura 12 – Band structure of MoTe-MoSe heterostructure with DOS per atom contributions from region 1 and 2.

large defect relative to the nanowire, we built a more extensive 240-atom supercell, integrating the 36 atoms from the MoSe defect into a large wire containing 204 atoms. In the MoTe-MoSe supercell, the results, displayed in Fig. 13, show even more dominance of the defect to flat bands near the Fermi level, reinforcing the interpretation that it is responsible for the emergence of these discrete levels in the gap region.

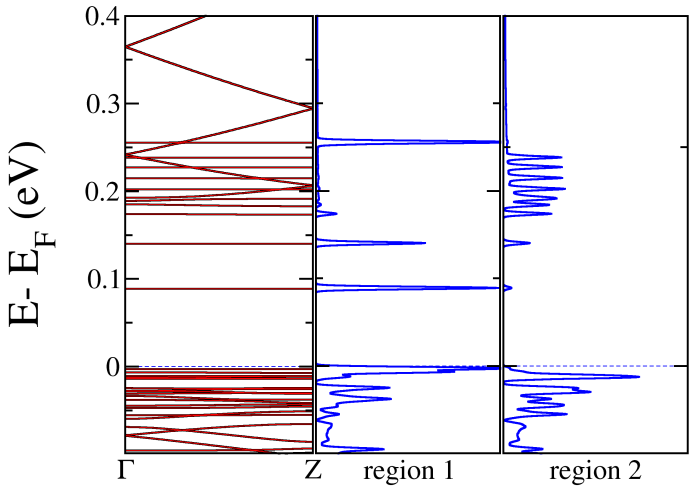

Figura 13 – Band structure of MoTe-MoSe extended heterostructure with DOS per atom contributions from region 1 and 2.

The physics behind the result can be better interpreted if we consider the metallic region

(MoSe segment) as a defect in the semiconducting MoTe nanowire. As it is well known, if defect introduce states into the gap region of a semiconductor, these states are localized within the defect region, which means that they present an exponential decay (spatially) away from the defect. Interestingly, discrete states spatially localized characterize the so-called quantum dots. Usually, they are produced via three-dimensional confinement. However, in low-dimensional systems, such as carbon nanotubes, the quantum dots behavior can be achieved by the intercalation of a small portion of a metallic nanotube into a semiconductor one, such as in the (6,4)/(5,5)/(6,4) junction proposed and theoretically investigated by L. Chico et. al. [30]. Similar behavior was predicted in the case of a bent semiconducting carbon nanotube [31]. In this case, the flattened bent region act as the "metallic"defect inserted into the semiconducting nanotube (by flattening the tube, a semiconductor-metal transition takes place.) Our proposal for the TMMs is similar, and our calculations indicate an analogous phenomenology, with discrete states separated by $\approx$ 0.1 eV.

In summary, the MoSe–MoTe hybrid system demonstrates that chemical and structural modulations in 1D TMM nanowires can induce confined electronic states. These discrete levels, arising from local discontinuities, highlight the potential of compositional engineering to tailor electronic properties in low-dimensional systems — a concept that will be further explored in the next section, which investigates how uniaxial strain in MoSe nanowires can drive a transition from metallic to semiconducting behavior as the lattice parameter increases.

3.3 Electronic Modulation by Uniaxial Strain in MoSe Nanowires

The manipulation of electronic properties through strain in transition-metal dichalcogenides has proven to be a promising path for flexible nanoelectronic devices [32] [33] [34]. Furthermore, specific investigations into transition-metal monochalcogenides present strain as a key factor in modulating stability and electronic properties [35]. MoTe nanowires synthesized within carbon nanotubes (CNTs) exhibit unique mechanical and electronic properties due to strain induced by confinement [14]. In this section, we are interested in the specific case of MoSe, whose metallic behavior was previously shown in this chapter, focusing on the effects of uniaxial stretching and compression, and the transition between metallic and semiconductor regimes.

Through DFT calculations, we analyzed how strain alters the behavior of MoSe nanowires, which have a relaxed wire lattice parameter of approximately 4.50 Å. The lattice parameter was varied from 3.90 Å to 5.20 Å, with the total energy of the system recorded to generate Fig. 14. As expected, the total energy of the nanowire is minimal when there is no strain and increases as we move away from the relaxed wire lattice parameter. In this process, an interesting behavior is observed: during the increase in strain, a transition from metal (4.90 Å) to semiconductor (5.00 Å) is observed.

As seen before (in Fig. 10), the relaxed MoSe nanowire exhibits a metallic character, with bands crossing the Fermi level, reflecting strong overlap between Mo-4d and Se-4p orbitals.

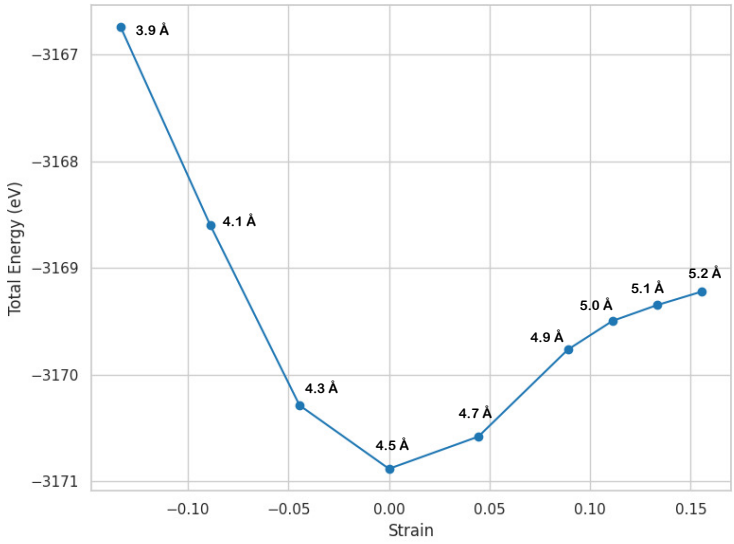

Figura 14 – Total energy as a function of applied uniaxial strain. Each marker is annotated with its corresponding lattice parameter in angstroms, ranging from 3.90 Å to 5.20 Å. The curve reaches a minimum in zero strain, indicating the equilibrium lattice constant.

With the increase to 4.90 Å (left panel in Fig. 15), a noticeable decrease in the density of states near the Fermi level is observed, indicating the progressive isolation of electronic states and the onset of gap opening toward a semiconductor regime. Finally, upon reaching 5.00 Å (right panel in Fig. 15), a clear separation between the valence band maximum (VBM) and the conduction band minimum (CBM) is observed, with a direct gap $\Delta E = 0.34$ eV at the Γ point, confirming the semiconductor character. The progressive expansion of the lattice parameter increases the Mo-Se interatomic distance, weakening the orbital interaction that sustains the metallic character. The narrowing of the DOS, observed from 4.51 Å to 4.90 Å, anticipates the isolation of states near the Fermi level. The transition to semiconductor at 5.00 Å reflects the point where orbital overlap can no longer sustain metallic transport, opening a direct gap of 0.34 eV.

The analysis reveals that 1D MoSe transitions from metallic to semiconductor under increasing uniaxial strain, with the transition occurring between 4.90 Å and 5.00 Å of the lattice parameter. This ability to modulate the gap through mechanical deformation opens up possibilities for "straintronics" in MoSe-based nanodevices, where conductivity can be controlled reversibly and precisely.

3.4 Influence of possible substrates on WTe Nanowires

TMMs nanowires have emerged as promising platforms for quantum applications due to their tunable electronic properties and low-dimensional confinement. Among them, WTe stands out as a narrow band-gap semiconductor. Recent studies reinforce its multifunctional versatility, addressing its electronic structure from first principles, quantum confinement and edge effects [6], electronic transport [15], and substrate-induced modulation [36]. Collectively,

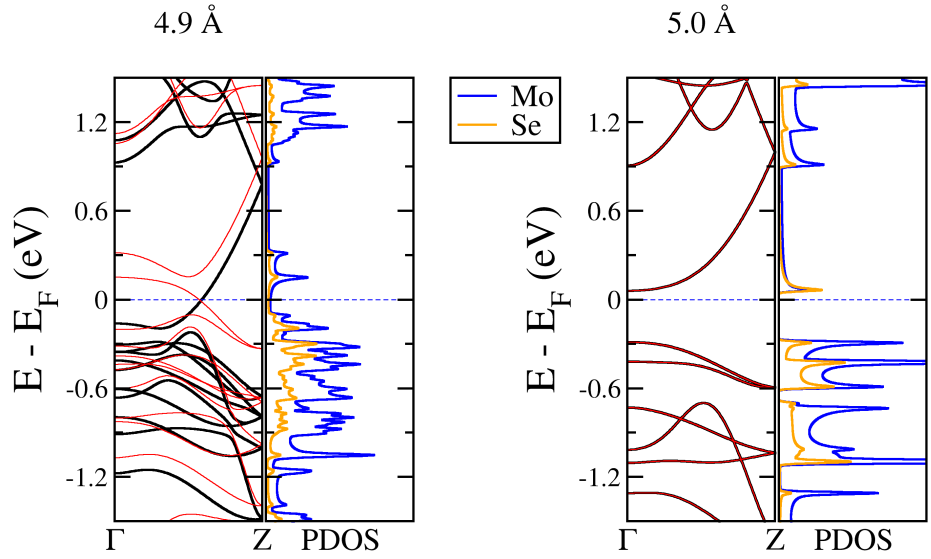

Figura 15 – Band structures of MoSe nanowire with 4.90 and 5.00 Å lattice parameter, showing the transition from metal to semiconductor.

these works position WTe as a robust and adaptable platform for quantum engineering.

Among the mechanisms capable of exploiting this versatility, proximity to specific substrates stands out, as they can act as sources of structural, electronic, or magnetic perturbation. In this section, we analyze three hybrid systems composed of WTe nanowires interacting via van der Waals with different materials: silane, PtS_2 monolayer, and CrI_3 monolayer. The minimum distance between WTe and the substrates is close to 3.50 Å. The analysis is based on band structure and DOS diagrams obtained from DFT calculations, which reveal how each substrate influences the electronic behavior of the nanowire in the vicinity of to the Fermi level.

3.4.1 Silane

In the first configuration, WTe interacts via van der Waals forces with silane molecules. Silane (SiH_4) is the simplest compound in the silicon hydride family, analogous to methane but with a silicon central atom. When functionalized, as in the case of the $Si_1O_3C_7H_{18}$ molecule (Fig. 16 a), oxygen atoms bond directly to silicon, forming Si-O bridges that enable connection with organic groups. Silane molecules are relevant in the present study because they may functionalize SiO_2 substrates, TMMs nanowires can then be deposited onto this platform and interact directly with these molecules. In the relaxed structure formed by WTe + silane, shown in Fig. 16 b, one silane molecule is positioned every two repetitions of the nanowire's unit cell. The corresponding band structure (Fig. 16 c) remains essentially unchanged compared to the isolated WTe nanowire, with gap opening between conduction and valence states. The DOS panel reveals that the states

in the Fermi level region are only from the WTe nanowire, with no relevant contributions from the silane. This indicates that silane can act as a passive substrate for WTe, with weak electronic interaction with WTe. The absence of significant polarization or interface states suggests that silane does not strongly perturb the system, allowing the nanowire to maintain its intrinsic characteristics. Such a configuration is advantageous in devices where the substrate should only provide mechanical support without interfering with electronic functionality.

The passive behavior of silane as a substrate has been widely explored in the context of self-assembled monolayers (SAMs), where organosilanes form stable covalent bonds with hydroxylated surfaces, enabling the deposition of thin films or nanostructures [37] [38]. In particular, functionalized silanes such as aminosilanes have been used to control the nucleation and growth of silicon nanowires [39]. These studies reinforce the role of silane derivatives not only as passive supports but also as active agents in the structural and electronic modulation of hybrid systems. Although commonly used as a neutral substrate, under certain conditions silane can actively interfere with the electronic structure of transition metal systems [40] [41]. Additionally, the use of organosilanes in pattern formation and selective growth of thin films has been demonstrated in studies of transition metal–silane complexes, which highlight how silane derivatives can influence bonding and surface interactions [37]. The versatility of silane chemistry thus supports its application in nanodevices where substrate properties must be finely tuned to preserve or enhance the functionality of the active material.

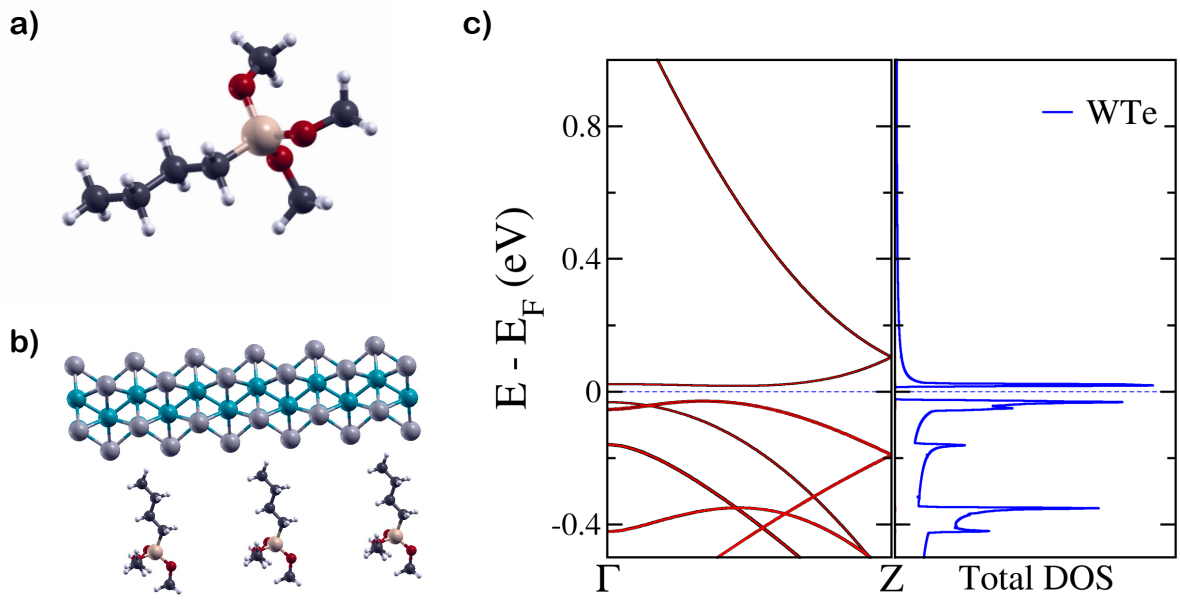

Figura 16 – a) Functionalized silane. White, black, red and pink spheres represent hydrogen, carbon, oxygen and silicon, respectively. b) WTe nanowire with functionalized silane, and c) its respective band structure and DOS panels. In the nanowire, cyan sphere represents W and gray represents Te.

3.4.2 PtS_2

Now, we investigated how the platinum disulfide (PtS_2) monolayer affects the characteristics of WTe nanowire. PtS_2, with top view shown in Figure 17a, is a 2D semiconductor material with an indirect gap (Fig. 17 c). The WTe–PtS_2 system is shown in Fig. 17 b. The combination of the two structures occurs with a wire length equal to 28.3 Å(six repetitions of the wire unit cell). Studies of heterostructures with PtS_2 indicate that it can act as a functional support, capable of modifying the electronic structure of the main material [42]. The WTe–PtS_2 presents signs of partial reorganization of electronic states, as seen in Fig. 17 d. The DOS panel shows that the bands near to Fermi level are dominated by WTe states. However, PtS_2 induces a spin splitting in the WTe bands with energy bands crossing the Fermi level. As the energy increases, the WTe contribution decreases, and in the range 0.55 to 1 eV, PtS_2 states dominate. It is important to emphasize that the DOS of PtS2 begins below the states associated with the 2D material, in the energy range of 0.50 eV in $\Gamma - Z$ path. This is due to chosen path, since we are interested in the properties of the wire and, consequently, what happens in the space reciprocal to its axis. The DOS captures all the states in this energy range of the Brillouin zone, so these states in the range 0.50 to 0.56 eV belong to points not shown in Fig. 17 d). Therefore, our calculations indicate that the interaction with PtS_2 strongly affects the electronic structure of WTe, inducing a metallic behavior and lifting spin degeneracies. Atomic Mulliken poputation analysis indicates a charge transfer of approximately 0.13 electrons per unit cell from WTe to PtS_2. Although moderate in magnitude, it is sufficient to shift the Fermi level of WTe and induce the spin splitting observed in the bands near the Fermi energy, underscoring the role of PtS_2 as a functional support capable of partially reorganizing the nanowire's electronic states.

3.4.3 CrI_3

Finally, we consider a WTe nanowire placed near a CrI_3 monolayer, a 2D ferromagnetic material (Fig. 18a) [43] [44]. CrI_3 can modulate the magnetic and electronic properties of adjacent materials through proximity effects and strain engineering [45] [46] [47]. Wu et al. [45] showed that CrI_3 monolayer exhibits strain-tunable magnetic and electronic properties, enabling control over neighboring systems. Wang et al. [46] explored heterostructures involving CrI_3 and other 2D materials, revealing its potential for band engineering and spin control in flexible devices. Yang et al. [47] demonstrated that adsorption of transition-metal atoms on CrI_3 monolayers enhances ferromagnetism and tunes electronic properties, reinforcing its role in spintronic applications. The combination between WTe and CrI_3, showed in Fig. 18b), occurs with a wire length equal to 14.95 Å(three repetitions of the wire unit cell). The band structure of CrI_3 (Fig. 18c) exhibits distinct spin channels, with energetically separated bands due to exchange coupling. In WTe–CrI_3 system (Fig. 18b), this interaction produces a pronounced spin polarization, significantly altering the WTe electronic structure (Fig. 18d). Both spin components now cross the Fermi level, resulting in substrate-induced metallic behavior. The Mulliken population analysis revels a charge transfer

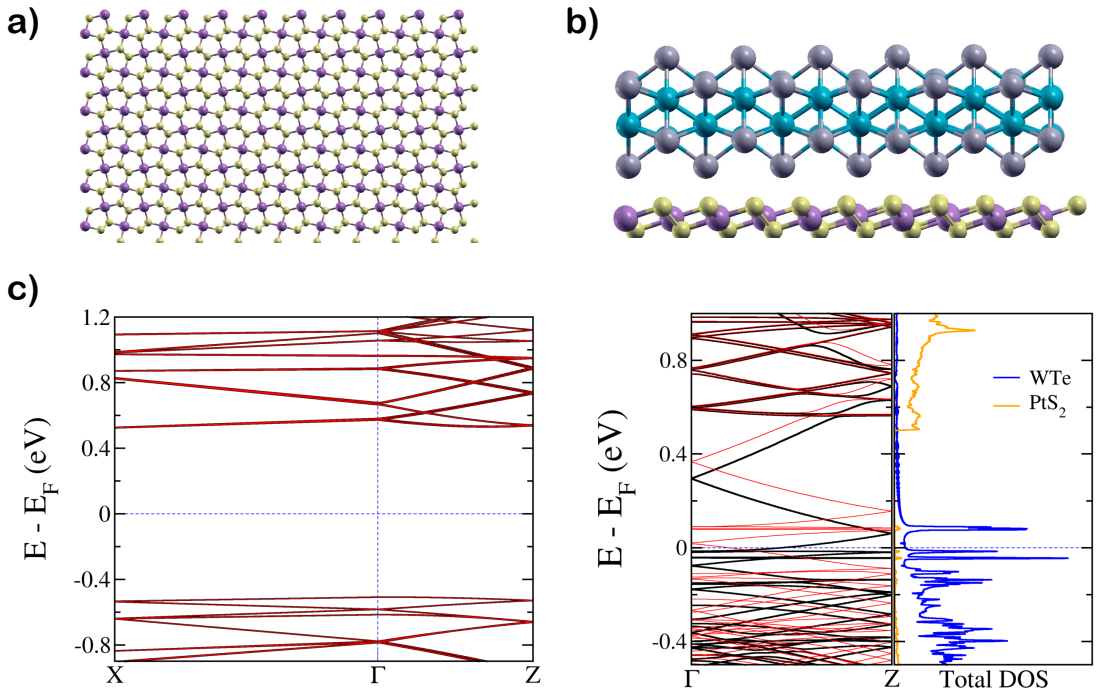

Figura 17 – a) PtS_2 monolayer with c) its respective band structure. Pink and yellow spheres represents platinum and sulfur, respectively. b) WTe nanowire with PtS_2. In the nanowire, cyan sphere represents W and gray represents Te. d) Band structure and DOS of WTe + PtS_2.

of about 0.03 electrons per unit cell from WTe to CrI_3. This modest yet non-negligible value supports the strong spin polarization imposed by the ferromagnetic substrate and explains the emergence of metallic behavior in both spin channels via proximity to CrI_3. The strong magnetic coupling enables control of carrier spin, opening possibilities for spin valves, magnetic memories, and qubits with tunable polarization.

3.4.4 Comparative analysis

The comparison between the three systems reveals how different substrates can selectively modulate the properties of WTe nanowires. Silane preserves the wire's original state, acting as a neutral support; PtS_2 induces metallicity and spin splitting; and CrI_3 imposes strong spin polarization, enabling magnetic functionalities, while also inducing transition to metallic state. These results demonstrate that substrate choice is not merely structural but a strategic parameter in quantum engineering, allowing the design of devices with tailored electronic and magnetic properties. Importantly, the results reinforces the versatility of TMM nanowires. In fact, they may present strong modulation of electronic ana magnetic properties induced by substrate effects.

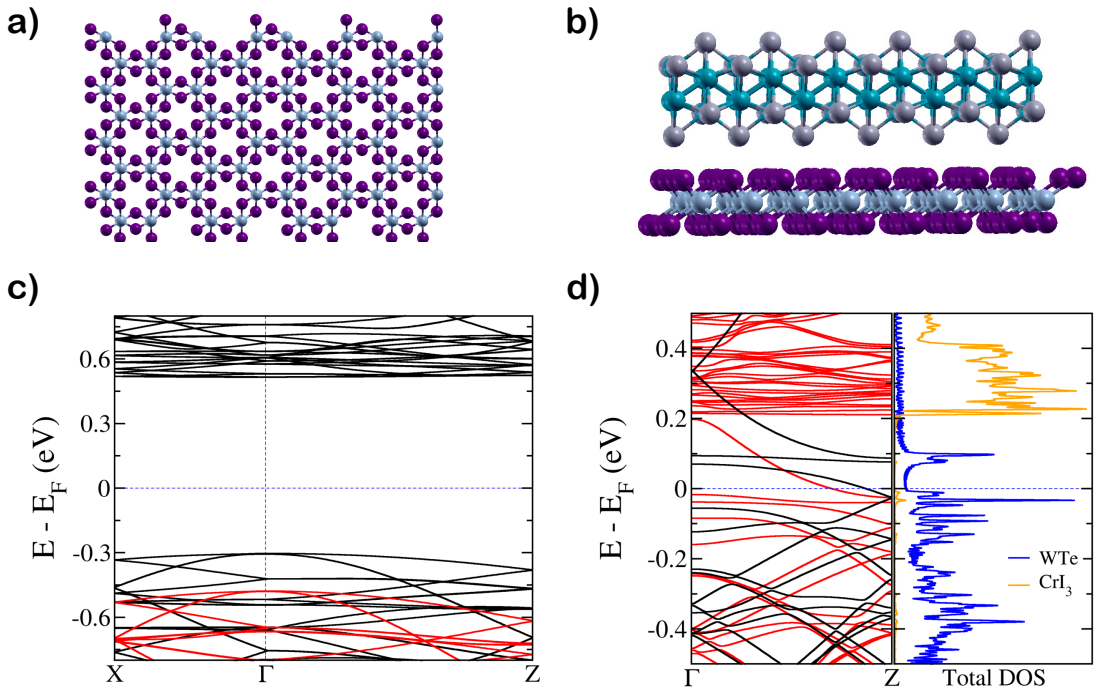

Figura 18 – a) CrI_3 monolayer with c) its respective band structure. Purple and blue spheres represents iodine and chromium, respectively. b) WTe nanowire with CrI_{23}. In the nanowire, cyan sphere represents W and gray represents Te. d) Band structure and DOS of WTe + CrI_3.

4 MOTE NANOWIRES ARRANGED IN HONEYCOMB AND KAGOME LATTICES

So far, the investigation of one-dimensional nanowire systems has revealed a wide range of electronic behaviors, strongly influenced by the composition, structural integrity, and surrounding environment. Metallic and semiconducting nanowires exhibit distinct conduction mechanisms, with band structures modulated by external factors such as strain, defects, and proximity to other materials. Imperfections like vacancies and distortions can introduce localized states or alter carrier mobility, while mechanical strain and nearby layers — such as functional substrates or magnetic monolayers — can induce band shifts, gap openings, or spin polarization splitting. These findings underscore the high tunability of 1D nanowire systems and their sensitivity to both intrinsic and extrinsic perturbations. Motivated by these insights, we now explore configurations in which nanowires are arranged into ordered two- and three-dimensional networks. Such architectures enable collective electronic phenomena driven by geometry, orbital overlap, and long-range coupling — even in the absence of direct covalent bonding.

In this context, MoTe nanowires have attracted intense attention due to their structural flexibility [9] , unique electronic properties [26], and potential in flexible electronics [14], spintronics [11], and catalysis [42]. Theoretical and experimental work has revealed that compositions such as MoTe can exist both in a pure 1D phase and in 1D/2D heterostructures, giving them versatility for integration into two- or three-dimensional networks [13] [15] [26]. Lim et al. [15] demonstrated via chemical vapor deposition (CVD) on sapphire substrates that MoTe nanowires can be grown into ordered 2D and 3D networks, revealing substantial electronic coupling between adjacent wires, even in the absence of covalent bonding. Their work highlights two fundamental insights: substrate-driven growth enables precise control over wire morphology, size, and orientation, and significant interwire hopping can emerge even in the absence of covalent bonds. Building on these findings, this chapter investigates the feasibility of realizing prototypical lattice electronic behaviors - Dirac cones and flat bands - in non-covalent MoTe assemblies. Using first-principles DFT calculations, we explore nanowires arranged in honeycomb and kagome geometries. By projecting the band structures onto the Mo-4d and Te-5p orbitals, we elucidate the pivotal role of spin–orbit coupling (SOC) in modulating orbital hybridization and electronic dispersion. Our results reveal that SOC-induced shifts generate distinct kagome manifolds and Dirac states, despite the absence of covalent interwire connections. These results were previously published on Journal of Physics: Condensed Matter [48].

Our first-principles approach is based on DFT [23,24] within the SIESTA implementation [25]. SIESTA makes use of norm-conserving pseudopotentials and double-zeta polarized (DZP) basis set - our basis includes 15 functions for Mo and 13 functions for Te. Exchange-correlation interactions are treated within the Generalized Gradient Approximation in the Perdew-Burke-Erzenholf parameterization (GGA-PBE) [27]. The geometries were optimized with a toleran ’ce in the maximum force component in any atom of $0.002\ eV$Å. To validate our results, selected

band structure calculations, including SOC, were replicated with Quantum Espresso [49–51] using a 75 Ry plane-wave cutoff and the same GGA-PBE functional, yielding excellent agreement with the SIESTA data.

4.1 Isolated nanowire, 2D and 3D arrangements

We begin with the basic MoTe nanowire arrangements described by H. E. Lim et al. [15], shown in Fig. 19: isolated wire, 2D and 3D lattices. The MoTe nanowire presents a lattice parameter along its axis of 4.63 Å, similar to that reported for wires grown inside CNTs [14] and those obtained from 2H-MoTe $_2$ [10]. As seen previously, we found a semiconducting behavior for the isolated wire, with an indirect band gap of $\approx 0.22\ eV$, as shown in Fig. 19. In contrast to isolated nanowire, the band structures of the 2D and 3D networks present a partially occupied conduction band. These two networks mentioned reveal an important aspect to our future discussion: the in-plane dispersions suggest relatively high interwire electronic hoppings, as it is particularly evident in the triangular case (3D). In the next sections, we show how this feature can be used to produce and modulate electronic states in other lattices.

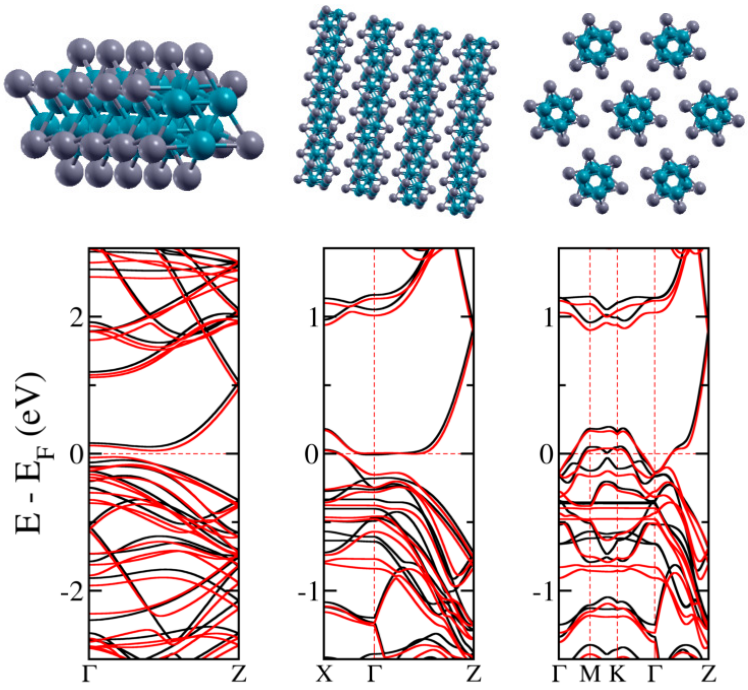

Figura 19 – Structures of transition-metal monochalcogenide systems: isolated nanowire, 2D and 3D lattices. The respective band structures are shown in the bottom panels. Cyan and gray spheres represent Mo and Te atoms, respectively. Band structures are presented without (red lines) and with (black lines) spin-orbit coupling.

4.2 Kagome lattice

First, we turn to the case in which the MoTe nanowires are arranged in a kagome lattice. We address the question on the possibility to achieve the kagome idiosyncrasies in the electronic behavior even in this non-covalent configuration. We considered the relaxed structure shown in Fig. 20(a), with the lattice parameter set to 22.10 Å. Given the substrate-driven growth of nanowires, we envisage a scenario in which such structures could be produced if the synthesis were conducted in association with specific molecules. These molecules would adhere to the substrate through van der Walls (vdW) forces and interact, also non-covalently, with the Te atoms of neighbor wires. As illustration, Fig. 20(b) shows that, for the choice of coronene as the auxiliary molecule, ideal vdW distances lead to a kagome structure with a lattice parameter equal to 22.10 Å.

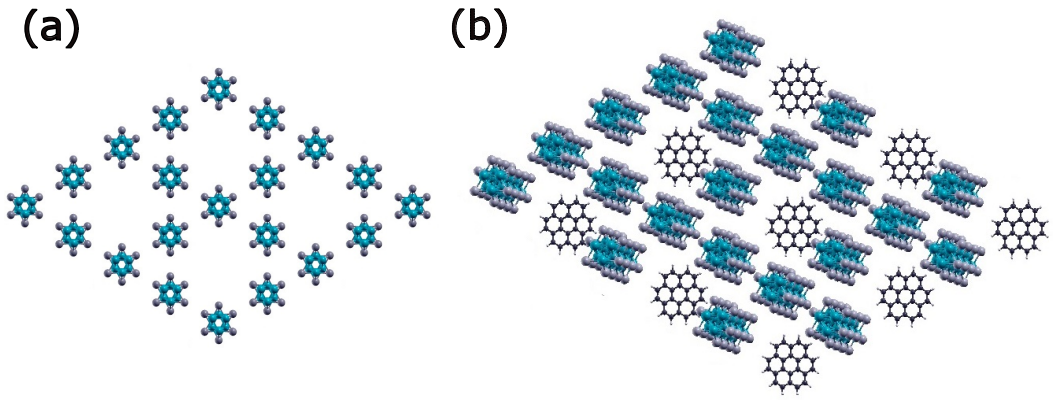

Figura 20 – (a) MoTe nanowires arranged in a kagome structure with a lattice parameter of 22.10 Å: cyan and gray circles represent Mo and Te atoms, respectively. (b) Schematic illustration of coronene molecules deposited on the substrate to assist nanowire growth in the kagome structure.

The question posed in the introduction of this chapter can now be answered with DFT electronic structure calculations including atomic relaxations and SOC interaction for the model lattice shown in Fig. 20(a). We focus our analyses on two-dimensional paths in the Brillouin zone. In the k_z direction, the dispersions will always be large due to the covalent bonds along the axis of the nanowires. The band structure, shown in Fig. 21, does reveal a pair of kagome manifolds clearly seen above and below the Fermi energy, which is set to zero. In the fatband scheme, orange and blue circles (lines) indicate contributions from Te p-orbitals and Mo d-orbitals, respectively. Therefore, the set of unoccupied kagome bands comes from Te orbitals; more specifically, as shown in the projected density of states (PDOS) presented in the right panel of Fig. 21, it is the in-plane p_x and p_y orbitals that are responsible for the largest contributions. On the other hand, the occupied manifold is mostly contributed by Mo d-orbitals, with minor hybridization with Te p-orbitals. Again, this aspect is quantified in the PDOS plot of the right panel: the in-plane Mo d-orbitals (d_{xy} and d_{x2-y2}) are the most important orbitals to these states.

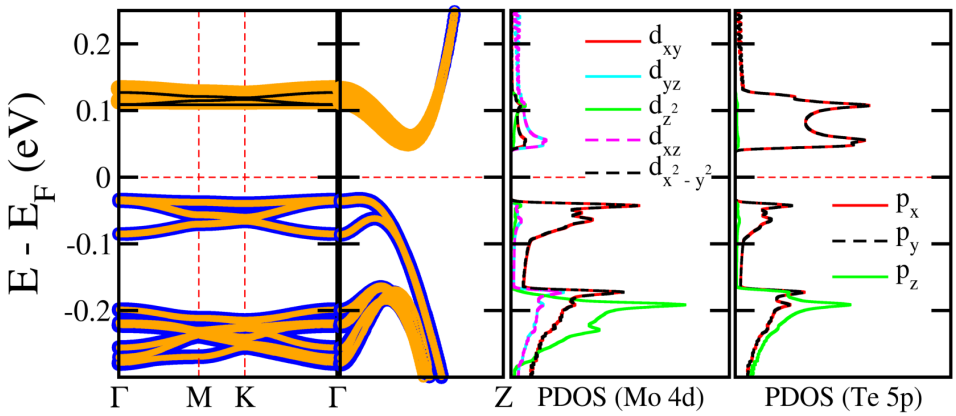

Figura 21 – Band structure and projection of the density of states for the nanowires arranged in kagome structure. The calculations include SOC and are presented in the fatband scheme. Orange and blue colors represent contributions from the Te-$5p$ and Mo-$4d$ orbitals, respectively. The PDOS scales (in arbitrary units) are the same in the two panels.

We devised a series of calculations to shed light on the above electronic structure. Firstly, we focused on the question “what is the role of spin-orbit interaction to the formation of the kagome bands?". The answer reveals an important aspect of the MoTe nanowire physics: the Mo d-orbital kagome set is completely originated from this interaction. Indeed, Fig. 22 shows the DFT band structure calculated without SOC. Concerning the kagome manifolds, there is no change in the Te p-bands in the conduction region, and a drastic effect in the Mo d-set, which, in fact, can no longer be identified. By comparing the projected density of states presented in the right panel of Fig. 22 with that of Fig. 21, it is reasonable to conclude that SOC induces an energy shift in the contributions originated from Mo in-plane states (d_{xy}, $d_{x^2-y^2}$), leaving unaffected those of d_{z^2}, in accordance with the intra-atomic SOC Hamiltonian

$$H_{SOC} = \sum_a \frac{\lambda_a}{\hbar} L_a \cdot S_a \,, \tag{4.1}$$

with atom index a and SOC coupling λ_a) and the fact that $m = 0$ for d_{z^2}, while $m = -2, 2$ for d_{xy} and $d_{x^2-y^2}$ [52]. Detached from d_{z^2} contributions, hybrid in-plane states become able to form unperturbed kagome states, as seen in the energy range from $-0.1\ to - 0.02\ eV$ of the band structure shown in Fig. 21. Comparing the band structures with and without SOC we can estimate the energy shifts in the range of 80 to 100 meV. Therefore, a first conclusion is that the Te in-plane p-orbitals form kagome states in the conduction band, while the Mo d-kagome manifold is SOC-induced in the valence region.

A second critical parameter is the distance between the individual wires, which defines the lattice parameter and controls the neighboring hopping magnitudes. As mentioned, the structure shown in Fig. 20 can be realized with a proper treatment of the substrate, possibly with inclusion of a molecule of the size of coronene during growth. If a slightly smaller molecule is used, the

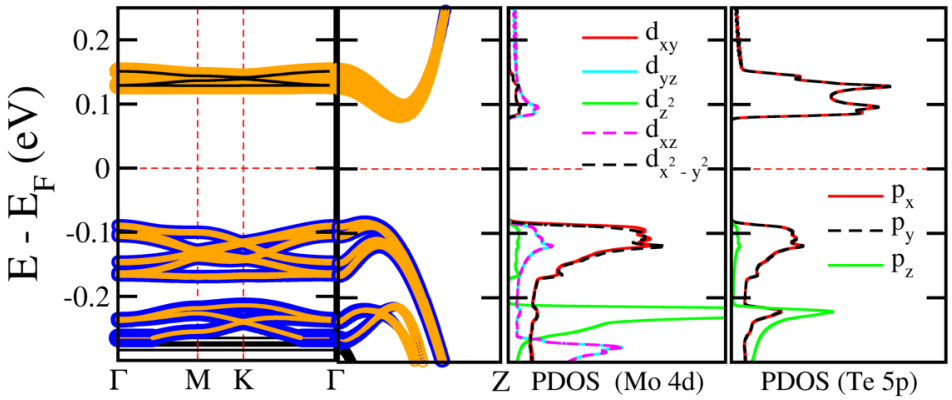

Figura 22 – Band structure (without SOC) and corresponding PDOS for the MoTe kagome structure with lattice parameter 22.10 Å. The PDOS scales are the same in the two panels. In the fatband scheme, orange and blue lines represent contributions from Te-$5p$ and Mo-$4d$ orbitals, respectively.

lattice parameter may be reduced to 18.44 Å, which corresponds to the equilibrium parameter for the MoTe nanowires in a kagome configuration. The smaller interwire distance brings important consequences to the electronic structure. As shown in Fig. 23(a) (without SOC), the two sets of kagome states, those originated from in-plane Te p- and Mo d-orbitals, are now found to be coupled. This is the result of a nonzero hopping between Te and Mo in-plane hybrid orbitals. By comparing Fig. 23(a) (wihout SOC) and (b) (with SOC), it becomes clear that the effect of SOC is particularly strong in the valence region. Distinct from the expanded lattice case of Fig. 21, the combination of additional hoppings and SOC which characterizes this case induces great distortions in the shape of Dirac and flat bands below the Fermi level. Shifts in the Mo d-contributions are accompanied by enhancement of dispersions even in portions dominated by Te p-orbitals (orange lines in the figure), which is the result of the strong hybridization between p and d orbitals.

So far, we have presented the results carried out with the SIESTA implementation of the DFT formalism. To ensure robustness to our results, we show, in Fig. 24, test calculations performed with the Quantum Espresso package, which makes use of a plane wave basis set. We choose two cases: MoTe nanowires arranged in a kagome lattice in the relaxed lattice parameter of 18.44 Å(left panel) and in the extended structure (right panel - lattice parameter of 22.10 Å). In both band structures, SOC is included. In fact, there is a remarkable agreement with Figs. 212(c) and 233(c), developed with the SIESTA implementation.

4.3 Honeycomb lattice

Now, we address the issue on the characterization of electronic states when the MoTe nanowires are arranged in a honeycomb structure. We applied basically the same methodology as before, combining relaxations with band structures calculations. For the structure represented

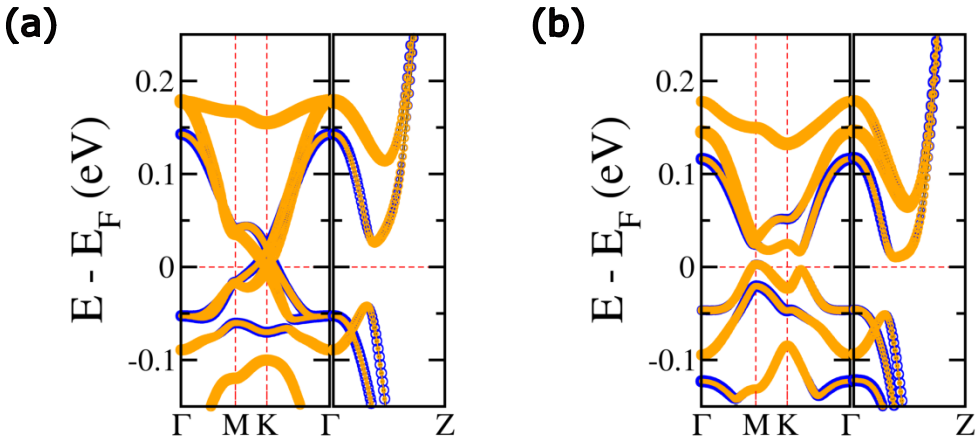

Figura 23 – (a) Band structure (without SOC) for the MoTe kagome structure with the relaxed lattice parameter of 18.44 Å. (b) Same as (c) expect for the inclusion of SOC. In the fatband scheme, orange and blue lines represent contributions from Te-$5p$ and Mo-$4d$ orbitals, respectively.

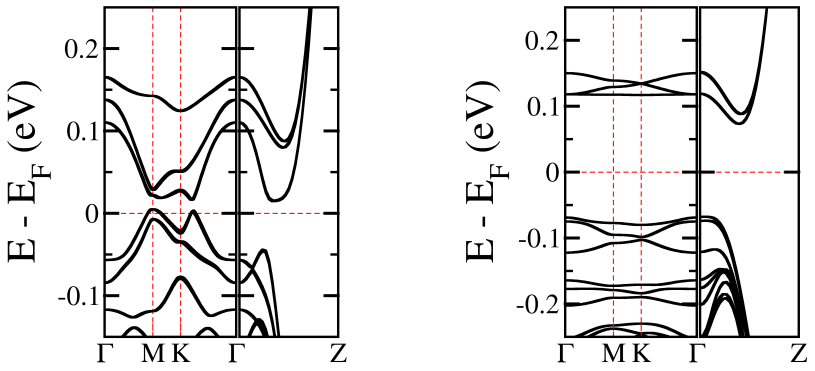

Figura 24 – Band structures (including SOC) for MoTe nanowires in kagome lattices with lattice parameter of 18.44 Å(left panel) and 22.10 Å(right panel).

in Fig. 25(a), we found a lattice parameter of 15.47 Å, resulting in minimal distances between nanowires of 3.55 Å. In Fig. 25(b), the band structure without SOC interaction reveals a pair of Dirac bands strongly concentrated in the Te p-orbitals, and the emergence of a flat band very close to the Fermi level. The flat band comes almost entirely from in-plane Mo d- and Te p-orbitals, with small contributions from Mo d_{z^2} orbitals. Fig. 25(c) details the electronic behavior upon inclusion of SOC interaction. As before, SOC affects the in-plane Mo d-orbitals, leaving unaffected the bands originated from Te. In fact, the Dirac point formed by the crossing of bands with p_x, p_y character can still be found at $E \sim 0.1\ eV$. However, SOC-induced energy shifts strongly alter the flat band, which acquires a dispersive feature, especially in the $\Gamma - M$ and $K - \Gamma$ directions. In the $M - K$ direction, the dispersion is relatively small, with a width of $0.01\ eV$, 80% smaller than that of the pair of Dirac bands.

How does this scenario change if the lattice is expanded? By increasing the lattice constant by $20\ \%$, we found the band structures shown in Fig. 26 (a) (without SOC) and (b) (with SOC). In

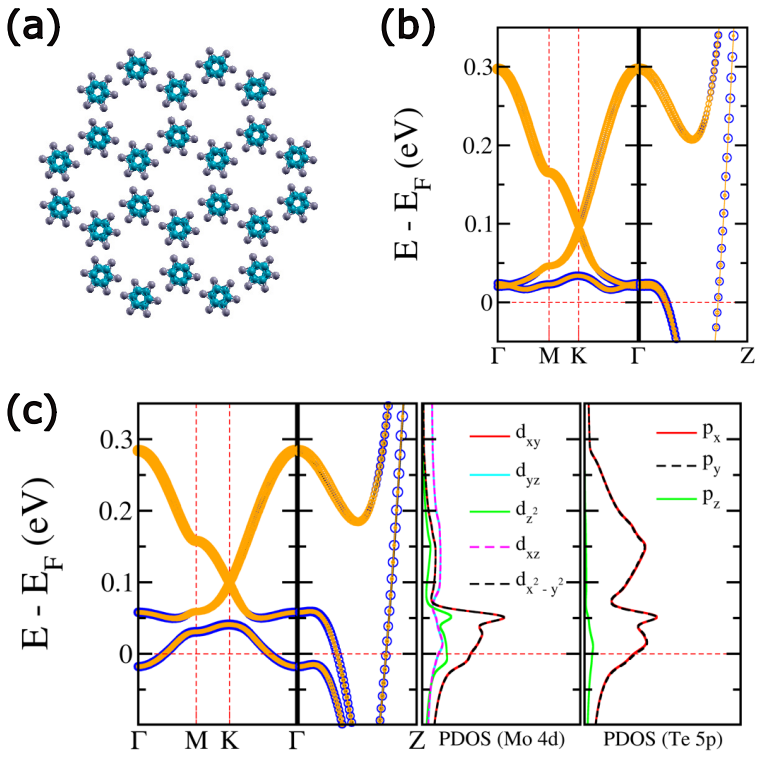

Figura 25 – (a) MoTe nanowires arranged in honeycomb structure with relaxed lattice parameter of 15.47 Å. (b) Corresponding band structure without SOC and (c) with SOC. In (c) the PDOS is also shown in the two right panels, both in the same scale. In the band structures, orange and blue lines of the fatband scheme indicate Te-$5p$ and Mo-$4d$ contributions, respectively.

the conduction band, both results indicate the pair of Dirac bands, almost exclusively originated from Te p-orbitals. Once again, the SOC effect is drastic in the Mo in-plane d-bands, which may be found in the occupied region of the spectrum. By introducing SOC, shifts in the in-plane Mo d-orbitals become responsible for a second set of Dirac bands that emerge in the valence region in the energy range from $\sim$ -0.1 eV to the Fermi level at zero energy. As before, we estimated the energy shifts to be in the range 80 to 100 meV. A small gap of $0.01\ eV$ is found at the K point separating the two bands of this manifold.

4.4 Conclusions

In summary, our calculations indicate that MoTe nanowires may be suitable building blocks to achieve typical electronic behaviors of specific lattices. These behaviors include Dirac states and flat bands. The relatively large hopping integrals, even in non-covalent configurations and which may be modulated by changing the interwire distance, and the spin-orbit coupling are important ingredients behind the phenomenology. The nanowire lattices offer the possibility of modulation of the electronic states by suitably doping the systems, which may be achieved by intercalating donor or acceptor atoms or molecules in the lattices.

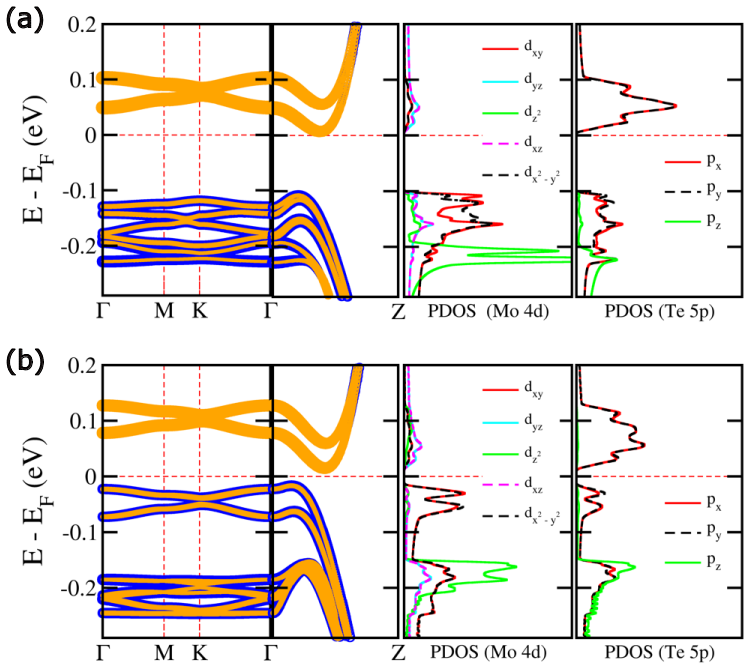

Figura 26 – Band structures and corresponding PDOS (a) with SOC and (b) without SOC for MoTe nanowires in an extended honeycomb structure (lattice parameter increased by 20% relative to the relaxed one). Orange and blue colors in the fatband scheme represent contributions from the Te-$5p$ and Mo-$4d$ orbitals, respectively. The PDOS scales (in arbitrary units) are the same in all plots.

5 GENERAL CONCLUSIONS

Throughout this thesis, we have conducted a comprehensive investigation into the structural and electronic properties of one-dimensional TMM nanowires, ranging from isolated systems to two- and three-dimensional arrangements with specific geometries, such as kagome and honeycomb networks. The approach combined first-principles calculations, structural relaxations, and detailed analyses of electronic band structures and projected densities of states, enabling direct correlations between chemical composition, lattice topology, and emergent electronic phenomena.

In Chapter3, we demonstrated that isolated nanowires exhibit a remarkable electronic duality: MoS and MoSe behave as genuine metals, whereas MoTe and WTe are narrow-gap indirect semiconductors, with gaps on the order of 0.1–0.2eV. This versatility stems from the choice of transition metal and chalcogen, allowing fine control over both the width and nature of the gap. We also explored a heterostructure consisting of a metallic MoSe segment embedded in a semiconducting MoTe matrix, where discrete, flat electronic states appear within the gap, localized in the metallic region and confined by the semiconducting host. This result highlights the potential of chemical and structural engineering to create localized states in 1D systems. Furthermore, we showed that uniaxial strain in MoSe nanowires can drive a controlled metal-to-semiconductor transition, with a direct gap of 0.34eV opening at $\approx 10\%$ elongation, demonstrating the feasibility of reversible "straintronic" devices. Finally, we examined the influence of different substrates on WTe nanowires: silane acts as a neutral support, preserving the intrinsic properties; PtS_2 maintains the band topology but induces spin splitting; and CrI_3 imposes strong spin polarization, turning WTe metallic and enabling spintronic functionalities.

In Chapter4, we advanced to ordered architectures of MoTe nanowires in 2D and 3D networks, showing that even without direct covalent bonds, these configurations can sustain phenomena typical of crystalline solids, such as Dirac cones and flat bands. In the kagome lattice, we found that the Mo d-orbital kagome manifold is entirely induced by spin–orbit coupling (SOC), while the Te p-orbital kagome states remain robust. Varying the lattice parameter strongly modulates p–d coupling, altering the shape and dispersion of flat bands and Dirac cones. In the honeycomb lattice, we observed the coexistence of Dirac bands and flat bands near the Fermi level, with SOC selectively affecting Mo d orbitals and potentially generating a second set of Dirac cones in the valence region. In both cases, inter-wire distance and lattice geometry proved to be critical parameters for controlling the electronic spectrum.

Taken together, the results of this thesis demonstrate that lattice topology, inter-wire spacing, and chemical composition are equally important control parameters in defining the electronic spectrum. Spin–orbit coupling emerges as a key element for inducing and tuning electronic states in nanowire-based architectures, and non-covalent arrangements can sustain complex electronic phenomena provided there is sufficient orbital overlap. These conclusions

not only deepen the fundamental understanding of low-dimensional systems but also point toward applications in electronics, spintronics, and quantum devices, where precise manipulation of Dirac states, flat bands, and spin–orbit interactions is desired. Future work may explore external fields, controlled doping, and interaction with functional substrates to further expand the accessible property space.

REFERÊNCIAS

[1] Chen, Jiancui, Zhang Zhou, Hongtao Liu, Ce Bian, Yuting Zou, Zhenyu Wang, Zhen Zhao, Kang Wu, Haitao Yang, Chengmin Shen, Zhi Gang Cheng, Lihong Bao e Hong Jun Gao: *One-dimensional weak antilocalization effect in 1T'-$MoTe_2$ nanowires grown by chemical vapor deposition*. Journal of Physics: Condensed Matter, 33(18):185701, apr 2021. Citado na página 10.

[2] Zhou, Ziyue, Ke Xu, Zixuan Song, Zhen Wang, Yanwen Lin, Qiao Shi, Yongchao Hao, Yuequn Fu, Zhisen Zhang e Jianyang Wu: *Isotope doping-induced crossover shift in the thermal conductivity of thin silicon nanowires*. Journal of Physics: Condensed Matter, 35(8):085702, dec 2022. Citado na página 10.

[3] Liu, Ying, Haifeng Lv e Xiaojun Wu: *Metal cyclopropenylidene sandwich cluster and nanowire: structural, electronic, and magnetic properties*. Journal of Physics: Condensed Matter, 33(23):235301, may 2021. Citado na página 10.

[4] Zhang, Wenqing, Juan Wang, Lanling Zhao, Junru Wang e Mingwen Zhao: *Transition-metal monochalcogenide nanowires: highly efficient bi-functional catalysts for the oxygen evolution/reduction reactions*. Nanoscale, 12:12883–12890, 2020. Citado 2 vezes nas páginas 10 e 11.

[5] Vilfan, I: *Mo_6S_6 nanowires: structural, mechanical and electronic properties*. The European Physical Journal B - Condensed Matter and Complex Systems, 51(2):277–284, maio 2006. Citado na página 10.

[6] Çakir, D., E. Durgun, O. Gülseren e S. Ciraci: *First principles study of electronic and mechanical properties of molybdenum selenide type nanowires*. Phys. Rev. B, 74:235433, Dec 2006. Citado 4 vezes nas páginas 10, 11, 25 e 31.

[7] Murugan, P., Vijay Kumar, Yoshiyuki Kawazoe e Norio Ota: *Assembling Nanowires from Mo-S Clusters and Effects of Iodine Doping on Electronic Structure*. Nano Letters, 7(8):2214–2219, 2007. Citado 2 vezes nas páginas 10 e 11.

[8] Murugan, P., Vijay Kumar, Yoshiyuki Kawazoe e Norio Ota: *Lithiated assemblies of metal chalcogenide nanowires*. Applied Physics Letters, 92(20):203112, maio 2008. Citado 2 vezes nas páginas 10 e 11.

[9] Shang, Chanjuan, Li Fu, Si Zhou e Jijun Zhao: *Atomic Wires of Transition Metal Chalcogenides: A Family of 1D Materials for Flexible Electronics and Spintronics*. JACS Au, 1(2):147–155, 2021. Citado 3 vezes nas páginas 11, 26 e 37.

[10] Zhu, Hui, Qingxiao Wang, Chenxi Zhang, Rafik Addou, Kyeongjae Cho, Robert M. Wallace e Moon J. Kim. Citado 4 vezes nas páginas 11, 12, 25 e 38.

[11] Liao, Lin, Keke Liu, Hao Luo, Yimeng Yu, Anan Guo, Weixiao Lin, Fanjie Xia, Qingjie Zhang, Xianli Su, Xinfeng Tang, Ning Wang e Jinsong Wu: *In Situ STEM Observation of Phase Transition Triggered by Mo Migration in $MoTe_2$*. ACS Nano, 18(46):31995–32002, 2024. Citado 2 vezes nas páginas 11 e 37.

[12] Lin, J., Cretu O. Zhou W. et al.: *Flexible metallic nanowires with self-adaptive contacts to semiconducting transition-metal dichalcogenide monolayers*. Nature Nanotech, 9:436–442, 2014. Citado na página 11.

[13] Lin, Junhao, Yuyang Zhang, Wu Zhou e Sokrates T. Pantelides: *Structural Flexibility and Alloying in Ultrathin Transition-Metal Chalcogenide Nanowires*. ACS Nano, 10(2):2782–2790, 2016. Citado 5 vezes nas páginas 11, 13, 25, 28 e 37.

[14] Nagata, Masataka, Shivani Shukla, Yusuke Nakanishi, Zheng Liu, Yung Chang Lin, Takuma Shiga, Yuto Nakamura, Takeshi Koyama, Hideo Kishida, Tsukasa Inoue, Naoyuki Kanda, Shun Ohno, Yuki Sakagawa, Kazu Suenaga e Hisanori Shinohara: *Isolation of Single-Wired Transition-Metal Monochalcogenides by Carbon Nanotubes*. Nano Letters, 19(8):4845–4851, 2019. Citado 6 vezes nas páginas 11, 14, 25, 30, 37 e 38.

[15] Lim, Hong En, Yusuke Nakanishi, Zheng Liu, Jiang Pu, Mina Maruyama, Takahiko Endo, Chisato Ando, Hiroshi Shimizu, Kazuhiro Yanagi, Susumu Okada, Taishi Takenobu e Yasumitsu Miyata: *Wafer-Scale Growth of One-Dimensional Transition-Metal Telluride Nanowires*. Nano Letters, 21(1):243–249, 2021. Citado 6 vezes nas páginas 11, 14, 25, 31, 37 e 38.

[16] Barreteau, C, F Ducastelle e T Mallah: *A bird's eye view on the flat and conic band world of the honeycomb and Kagome lattices: towards an understanding of 2D metal-organic frameworks electronic structure*. Journal of Physics: Condensed Matter, 29(46):465302, oct 2017. Citado 5 vezes nas páginas 16, 17, 18, 19 e 20.

[17] Ni, Xiaojuan, Yinong Zhou, Gurjyot Sethi e Feng Liu: *π-Orbital Yin–Yang Kagome bands in anilato-based metal–organic frameworks*. Phys. Chem. Chem. Phys., 22:25827–25832, 2020. Citado na página 18.

[18] Okamoto, Satoshi, Narayan Mohanta, Elbio Dagotto e DN Sheng: *Topological flat bands in a kagome lattice multiorbital system*. Communications Physics, 5(1):198, 2022. Citado na página 18.

[19] Kang, Mingu, Shiang Fang, Linda Ye, Hoi Chun Po, Jonathan Denlinger, Chris Jozwiak, Aaron Bostwick, Eli Rotenberg, Efthimios Kaxiras, Joseph G Checkelsky *et al.*: *Topological flat bands in frustrated kagome lattice CoSn*. Nature communications, 11(1):4004, 2020. Citado na página 18.

[20] Meier, William R., Mao Hua Du, Satoshi Okamoto, Narayan Mohanta, Andrew F. May, Michael A. McGuire, Craig A. Bridges, German D. Samolyuk e Brian C. Sales: *Flat bands in the CoSn-type compounds*. Phys. Rev. B, 102:075148, Aug 2020. Citado na página 18.

[21] Wu, Congjun, Doron Bergman, Leon Balents e S. Das Sarma: *Flat Bands and Wigner Crystallization in the Honeycomb Optical Lattice*. Phys. Rev. Lett., 99:070401, Aug 2007. Citado 2 vezes nas páginas 18 e 19.

[22] Wu, Congjun e S. Das Sarma: $p_{x,y}$*-orbital counterpart of graphene: Cold atoms in the honeycomb optical lattice*. Phys. Rev. B, 77:235107, Jun 2008. Citado 2 vezes nas páginas 18 e 19.

[23] Hohenberg, P. e W. Kohn: *Inhomogeneous Electron Gas*. Phys. Rev., 136:B864–B871, Nov 1964. Citado 3 vezes nas páginas 21, 25 e 37.

[24] Kohn, W. e L. J. Sham: *Self-Consistent Equations Including Exchange and Correlation Effects*. Phys. Rev., 140:A1133–A1138, Nov 1965. Citado 3 vezes nas páginas 21, 25 e 37.

[25] Soler, José M, Emilio Artacho, Julian D Gale, Alberto García, Javier Junquera, Pablo Ordejón e Daniel Sánchez-Portal: *The SIESTA method for ab initio order-N materials simulation*. J. Phys.: Condens. Matter., 14(11):2745, mar 2002. Citado 3 vezes nas páginas 23, 25 e 37.

[26] Yu, Yayun, Guang Wang, Yuan Tan, Nannan Wu, Xue Ao Zhang e Shiqiao Qin: *Phase-Controlled Growth of One-Dimensional Mo_6Te_6 Nanowires and Two-Dimensional $MoTe_2$ Ultrathin Films Heterostructures*. Nano Letters, 18(2):675–681, 2018. PMID: 29262252. Citado 2 vezes nas páginas 25 e 37.

[27] Perdew, John P., Kieron Burke e Matthias Ernzerhof: *Generalized Gradient Approximation Made Simple*. Phys. Rev. Lett., 77:3865–3868, Oct 1996. Citado 2 vezes nas páginas 25 e 37.

[28] Wang, Xuan, Akang Chen, Xinlei Wu, Jiatao Zhang, Jichen Dong e Leining Zhang: *Synthesis and Modulation of Low-Dimensional Transition Metal Chalcogenide Materials via Atomic Substitution*. Nano-Micro Letters, 16(1):163, março 2024. Citado na página 27.

[29] Rehman, Zia ur, Wen Zhu, Sheng Wang, Yijie Niu, Zahir Muhammad, Oyawale Adetunji Moses, Chuanqiang Wu, Muhammad Habib, Shuangming Chen, Xiaojun Wu, Zhe Sun, Pulickel M. Ajayan e Li Song: *Selective Selenium-Substituted Metallic MoTe2 toward Ternary Atomic Layers with Tunable Semiconducting Character*. The Journal of Physical Chemistry C, 123(40):24927–24933, 2019. Citado na página 27.

[30] Chico, L., M. P. López Sancho e M. C. Muñoz: *Carbon-Nanotube-Based Quantum Dot*. Phys. Rev. Lett., 81:1278–1281, Aug 1998. Citado na página 30.

[31] Mazzoni, M. S. C. e H. Chacham: *Atomic restructuring and localized electron states in a bent carbon nanotube: A first-principles study*. Phys. Rev. B, 61:7312–7315, Mar 2000. Citado na página 30.

[32] Island, Joshua O., Agnieszka Kuc, Erik H. Diependaal, Rudolf Bratschitsch, Herre S. J. van der Zant, Thomas Heine e Andres Castellanos-Gomez: *Precise and reversible band gap tuning in single-layer $MoSe^2$ by uniaxial strain*. Nanoscale, 8:2589–2593, 2016. Citado na página 30.

[33] Carrascoso, Felix, Hao Li, Riccardo Frisenda e Andres Castellanos-Gomez: *Strain engineering in single-, bi- and tri-layer MoS^2, $MoSe^2$, WS^2 and WSe^2*. Nano Research, 14(6):1698–1703, junho 2021. Citado na página 30.

[34] Costa, Ana Luiza Mariano Torres: *Propriedades eletrônicas e de transporte em nanoestruturas de metais de transição dicalcogenados*. Tese de Doutoramento, Universidade Federal do Ceará, 2019. Citado na página 30.

[35] Jin, Kyung Hwan e Feng Liu: *1D topological phases in transition-metal monochalcogenide nanowires*. Nanoscale, 12:14661–14667, 2020. Citado na página 30.

[36] Deng, Jinghao, Da Huo, Yusong Bai, Yanping Guo, Zemin Pan, Shuangzan Lu, Ping Cui, Zhenyu Zhang e Chendong Zhang: *Precise Tuning of Band Structures and Electron Correlations by van der Waals Stacking of One-dimensional W_6Te_6 Wires*. Nano Letters, 20(12):8866–8873, 2020. Citado na página 31.

[37] Ulman, Abraham: *Formation and Structure of Self-Assembled Monolayers*. Chemical Reviews, 96(4):1533–1554, 1996. PMID: 11848802. Citado na página 33.

[38] Prime, Kevin L. e George M. Whitesides: *Self-Assembled Organic Monolayers: Model Systems for Studying Adsorption of Proteins at Surfaces*. Science, 252(5009):1164–1167, 1991. Citado na página 33.

[39] Schmidt, Volker, Joerg V. Wittemann, Stephan Senz e Ulrich Gösele: *Silicon Nanowires: A Review on Aspects of their Growth and their Electrical Properties*. Advanced Materials, 21(25-26):2681–2702, 2009. Citado na página 33.

[40] Cabrera, A L, J F Kirner e J N Armor: *Oxidation protection for a variety of transition metals and copper via surface silicides formed with silane containing atmospheres*. Journal of Materials Research, 6(1):71–79, janeiro 1991. Citado na página 33.

[41] Tarczay, György, Marko Förstel, Pavlo Maksyutenko e Ralf I. Kaiser: *Formation of Higher Silanes in Low-Temperature Silane (SiH_4) Ices*. Inorganic Chemistry, 55(17):8776–8785, 2016. Citado na página 33.

[42] Zhang, Li, Kai Ren, Haiyan Cheng, Zhen Cui e Jianping Li: *The First-Principles Study of External Strain Tuning the Electronic and Optical Properties of the 2D $MoTe_2/PtS_2$ van der Waals Heterostructure*. Frontiers in Chemistry, Volume 10 - 2022, 2022, ISSN 2296-2646. Citado 2 vezes nas páginas 34 e 37.

[43] Huang, Bevin, Genevieve Clark, Efrén Navarro-Moratalla, Dahlia R Klein, Ran Cheng, Kyle L Seyler, Ding Zhong, Emma Schmidgall, Michael A McGuire, David H Cobden, Wang Yao, Di Xiao, Pablo Jarillo-Herrero e Xiaodong Xu: *Layer-dependent ferromagnetism in a van der Waals crystal down to the monolayer limit*. Nature, 546(7657):270–273, junho 2017. Citado na página 34.

[44] Lado, J L e J Fernández-Rossier: *On the origin of magnetic anisotropy in two dimensional CrI_3*. 2D Materials, 4(3):035002, jun 2017. Citado na página 34.

[45] Wu, Zewen, Jin Yu e Shengjun Yuan: *Strain-tunable magnetic and electronic properties of monolayer CrI_3*. Phys. Chem. Chem. Phys., 21:7750–7755, 2019. Citado na página 34.

[46] Wang, Qian, Nannan Han, Xuyang Zhang, Chenhui Zhang, Xixiang Zhang e Yingchun Cheng: *Modulation of electronic and magnetic properties of monolayer chromium trihalides by alloy and strain engineering*. Journal of Applied Physics, 129(15):155104, abril 2021, ISSN 0021-8979. Citado na página 34.

[47] Yang, Qiang, Xiaohui Hu, Xiaodong Shen, Arkady V. Krasheninnikov, Zhongfang Chen e Litao Sun: *Enhancing Ferromagnetism and Tuning Electronic Properties of CrI_3 Monolayers by Adsorption of Transition-Metal Atoms*. ACS Applied Materials & Interfaces, 13(18):21593–21601, 2021. PMID: 33904708. Citado na página 34.

[48] Oliveira, Túlio V de, Guilherme A S Ribeiro e Mario S C Mazzoni: *Investigation of MoTe nanowires in honeycomb and kagome lattices: Dirac cones and flat bands*. Journal of Physics: Condensed Matter, 37(14):145502, feb 2025. `https://dx.doi.org/10.1088/1361-648X/adb5e6`. Citado na página 37.

[49] Giannozzi, P, O Andreussi, T Brumme, O Bunau, M Buongiorno Nardelli, M Calandra, R Car, C Cavazzoni, D Ceresoli, M Cococcioni, N Colonna, I Carnimeo, A Dal Corso, S de Gironcoli, P Delugas, R A DiStasio Jr, A Ferretti, A Floris, G Fratesi, G Fugallo, R Gebauer, U Gerstmann, F Giustino, T Gorni, J Jia, M Kawamura, H Y Ko, A Kokalj, E Küçükbenli, M Lazzeri, M Marsili, N Marzari, F Mauri, N L Nguyen, H V Nguyen, A Otero de-la Roza, L Paulatto, S Poncé, D Rocca, R Sabatini, B Santra, M Schlipf, A P Seitsonen, A Smogunov, I Timrov, T Thonhauser, P Umari, N Vast, X Wu e S Baroni: *Advanced capabilities for materials modelling with QUANTUM ESPRESSO*. Journal of Physics: Condensed Matter, 29(46):465901, 2017. Citado na página 38.

[50] Giannozzi, Paolo, Stefano Baroni, Nicola Bonini, Matteo Calandra, Roberto Car, Carlo Cavazzoni, Davide Ceresoli, Guido L Chiarotti, Matteo Cococcioni, Ismaila Dabo, Andrea

Dal Corso, Stefano de Gironcoli, Stefano Fabris, Guido Fratesi, Ralph Gebauer, Uwe Gerstmann, Christos Gougoussis, Anton Kokalj, Michele Lazzeri, Layla Martin-Samos, Nicola Marzari, Francesco Mauri, Riccardo Mazzarello, Stefano Paolini, Alfredo Pasquarello, Lorenzo Paulatto, Carlo Sbraccia, Sandro Scandolo, Gabriele Sclauzero, Ari P Seitsonen, Alexander Smogunov, Paolo Umari e Renata M Wentzcovitch: *QUANTUM ESPRESSO: a modular and open-source software project for quantum simulations of materials*. Journal of Physics: Condensed Matter, 21(39):395502 (19pp), 2009. Citado na página 38.

[51] Giannozzi, Paolo, Oscar Baseggio, Pietro Bonfà, Davide Brunato, Roberto Car, Ivan Carnimeo, Carlo Cavazzoni, Stefano de Gironcoli, Pietro Delugas, Fabrizio Ferrari Ruffino, Andrea Ferretti, Nicola Marzari, Iurii Timrov, Andrea Urru e Stefano Baroni: *Quantum ESPRESSO toward the exascale*. The Journal of Chemical Physics, 152(15):154105, 2020. Citado na página 38.

[52] Ridolfi, E, D Le, T S Rahman, E R Mucciolo e C H Lewenkopf: *A tight-binding model for MoS_2 monolayers*. Journal of Physics: Condensed Matter, 27(36):365501, aug 2015. Citado na página 40.